CHALMERS

Development and Investigation of a Safety Product Concept for E-Vehicle Battery Systems

The Development of an Emergency Cooling Spray-on System and the Test Method to Evaluate Its Performance

Master's Thesis in Automotive Engineering

PER GUSTAFSSON

LINUS LINDGREN

Development and Investigation of a Safety Product Concept for E-Vehicle Battery Systems

The Development of an Emergency Cooling Spray-on System and the Test Method to Evaluate Its Performance

PER GUSTAFSSON

LINUS LINDGREN

Development and Investigation of a Safety Product Concept for E-Vehicle Battery Systems
The Development of an Emergency Cooling Spray-on System and the Test Method to Evaluate Its Performance
PER GUSTAFSSON

LINUS LINDGREN

Cover:
Figure is displaying a spray mist created from forcing high pressurized liquid through a PJ nozzle.

Development and Investigation of a Safety Product Concept for E-Vehicle Battery Systems

The Development of an Emergency Cooling Spray-on System and the Test Method to Evaluate Its Performance

Master's Thesis in *Master's Thesis in Automotive Engineering*

PER GUSTAFSSON

LINUS LINDGREN

Department of Applied Mechanics

Division of Vehicle Safety

Chalmers University of Technology

ABSTRACT

There are three major types of abuse mechanisms when considering potential root causes for critical failure events of vehicle traction battery systems. All three may result in thermal runaway, i.e. exothermal decomposition of active materials inside battery cells unless any countermeasures are set in place.

The focus in this report is to develop a safety system concept to prevent thermal runaway and a methodology to evaluate the performance of it. This report begins with a review of already existing safety systems. Based on the review, a safety system concept was developed followed by the development of a test rig to measure the cooling power of a spray-on cooling system; its functionality is presented in this report.

The spray-on cooling system in this study is tested through physical experiments with two different cooling mediums:

- Pure water mist
- A mixture of 25% Ammonia(NH_3)/75% Water(H_2O) being applied as a mist

Two spray nozzles with different nozzle hole diameters are also compared in terms of their relative influence on the cooling efficiency, i.e. how the droplet size (which is affected by the nozzle hole diameter and spray pressure) affects cooling performance. A smaller nozzle at a given pressure will result in smaller droplets.

Prior to physical testing, the cooling mediums' cooling performance was evaluated based on latent heat of evaporation using the software Aspen Plus V7.3. The simulation results were then examined and validated by the physical experiments. The results generated presented that the 25% NH_3/75% H_2O mixture mist was 18.6% more efficient in cooling than pure water mist in a spray-on cooling system when considering temperatures between 90-150°C.

Additionally, the freezing point of the mixture was evaluated using a temperature chamber, and the results proved that a mixture of 25% NH_3/75% H_2O can withstand at least -43°C before freezing.

Tests with the two different spray nozzle diameters, provided that the cooling power of the larger was slightly higher. However the spray duration was increased by 294% using the smaller nozzle diameter instead of the larger. Based on these result it was concluded that the smaller nozzle diameter allowed for approximately 19.5% more energy to be absorbed than the larger, given a specific volume of cooling medium.

Key words: Lithium-Ion Battery, Emergency Cooling, Ammonia/Water Mixture

Utveckling och undersökning av ett produktsäkerhetskoncept för E-fordons batterisystem

Utvecklingen av ett akutkylningssystem och en testmetod för att evaluera dess prestanda.

Examensarbete inom fordonsteknik

PER GUSTAFSSON

LINUS LINDGREN

Institutionen för tillämpad mekanik

Avdelningen för Skadeprevention

Chalmers tekniska högskola

SAMMANFATTNING

Det finns tre huvudsakliga typer av skademekanismer när fokus ligger på kritiska skador som kan förekomma på batterisystem avsedda för framdrivning av fordon – mekaniskt, elektriskt och termiskt våld. Alla tre innebär att battericellernas interna temperatur ökar vilket kan leda till termisk rusning, dvs. exoterm nedbrytning av aktiva material inuti battericeller om inga motåtgärder vidtas tidigt.

Denna rapport fokuserar inledningsvis på att undersöka redan befintliga säkerhetssystem; vidare presenteras en problemställning och ett problemlösande säkerhetssystemskoncept samt en metod för att utvärdera prestandan hos detta. För att utvärdera lösningen har en testrigg tagits fram. Med hjälp av testriggen är det möjligt att härleda kyleffekten från ett akutkylningssystem vilket åstadkoms genom temperaturmätningar. Prestandan på kylsystemet i denna studie testas genom fysiska experiment med två olika kylmedier:

- Vattendimma
- En blandning av 25 % Ammoniak (NH_3) / 75 % Vatten (H_2O) i form av en dimma.

Två munstycken med olika diameter på munstyckshålen har även jämförs i termer av deras relativa inflytande på kyleffekten, dvs. hur droppstorleken (som är beroende av munstyckshålets diameter och spraytryck) påverkar kyleffekten. Ett mindre munstyckshål vid ett givet tryck resulterar i mindre droppstorlek.

Innan de fysiska testerna kunde genomföras utvärderades kyleffekten baserad på det latenta förångningsvärmet genom simuleringsmjukvaran Aspen Plus v7.3. Simuleringsresultaten undersöktes och jämfördes sedan med de fysiska experimenten.

Resultaten visade att 25 % NH_3/75 % H_2O blandning i form av en dimma erbjöd 18,6 % högre kyleffektivitet än vattendimma när man undersöker temperaturer mellan 90-150°C.

Fryspunkten för blandningen utvärderades med hjälp av en klimatkammare, vilket visade att en blandning av 25 % NH_3/75 % H_2O har en fryspunkt under -43° C.

Tester av de två olika dimmunstyckena med olika munstycksdiameter visade att kyleffekten vid användandet av det med större munstycksdiameter är lite högre. Dock ökade spraydurationen med 294 % vid användandet av det mindre munstycket istället för det större. Utifrån dessa resultat drogs slutsatsen att det mindre munstycket möjliggör att cirka 19,5% mer energi kan absorberas jämfört med det större, givet en specifik volym av kylmedium.

Nyckelord: Litiumjonbatteri, akutkylning, ammoniak/vatten-blandning

II

Contents

Preface

In this study, investigations regarding whether ammonia/water mixture can be used as a spray-on cooling medium has been conducted. The project has been carried out from February 2013 to September 2013. The project is part of a Master's of Science in Engineering. The project is carried out at the Department of Applied Mechanics, Division of Vehicle Safety at Chalmers University of Technology, Sweden. The project has been conducted at Autoliv Development AB and Chalmers University of Technology.

The means needed to conduct this project has been provided by Autoliv Development AB. We would like to thank David Sturk, M.Sc.Ch.Eng. at Autoliv Development AB for being the supervisor and our mentor throughout this project.

We would also like to thank Johan Davidsson at Chalmers University of Technology for being the examiner of this Master's Thesis.

We would also like to thank Prof. Lennart Vamling at Chalmers University of Technology for his knowledge and guidance in chemical simulations.

Finally, the physical tests could never have been conducted without the professional help from the staff at Autoliv, Vårgårda.

Göteborg September 2013

Per Gustafsson

Linus Lindgren

Notations

C-Rate Time to fully discharge/charge battery to empty/full charge [1/h]

$$C-Rate = \frac{current\ [A]}{electric\ capacity\ [Ah]}$$

NCA Lithium Nickel Cobalt Aluminum Oxide
NMC Lithium Nickel Manganese Cobalt Oxide
$LiFePO_4$ Lithium Iron Phosphate
$LiPF_6$ Lithium Hexafluorophosphate
HSU Heat Storage Unit
PCM Phase Change Material
E-Vehicles Electrically Driven Vehicle
SEI Solid Electrolyte Interface
SOC State of Charge
BMS Battery Management System
IDLH Immediately Dangerous to Life and Health
NIOSH National Institute for Occupational Safety and Health

1 Introduction

This section aims to aid the reader understand the purpose of the project. The project is conducted as a collaboration between Autoliv Research AB and Chalmers University of Technology as a master thesis within Automotive Engineering.

1.1 Research Approach

The work conducted throughout this project is based on literature studies which were carried out in order to gain deeper knowledge about the given problem and its origin, i.e. batteries may fail violently if subjected to abusive conditions such as mechanical, electrical and thermal abuse.

This report presents an innovation process with a final concept validation. This process started with a literature survey gathering scientific information for deeper knowledge of the given subject. On basis of such knowledge a problem description was defined as well as a concept solution. In order to validate this concept solution a test rig was constructed and tests were performed. The test results were investigated so as to conclude if the selected concept would present a relevant safety enhancement if being used in a vehicle battery system.

1.2 Background

The two primary propellants used in vehicles today are gasoline and diesel. Being fossil fuels the use results in high net production of carbon dioxide as well as depletion of fossil resources. The depletion of resources in combination with increasing temperature around the globe, due to the carbon dioxide's properties as a greenhouse gas, results in the need of a CO2-smart vehicle fleet. Using electric vehicles and hybrid electric vehicles greatly reduces the CO2 emissions.(Place, 2011)

There are several types of batteries available on the market for Electrically Driven Vehicles (E-Vehicles). The most promising types at this time are the batteries based on Lithium-ion (Li-ion) chemistries. They possess high energy density and relatively high power density (Sturk, 2012). However, electric vehicles are accompanied by new safety issues; i.e. electric safety, thermal management and structural solutions to protect the battery.

Introducing a Li-ion battery into an already cramped vehicle must not jeopardize the crashworthiness; the aforementioned new safety issues must be addressed.

There are three main battery abuse mechanisms: electrical abuse, thermal abuse and mechanical abuse. Examples of electrical abuse are short-circuiting and over-charging the battery. Thermal abuse is the result of high temperatures within the battery. Sources of temperature increase can be either external fire or internal short-circuit (i.e. joule-heating). Mechanical abuse is either puncturing, mechanically shocking, denting or pinching the battery which all could result in short-circuit and thereby an increase in temperature (Sehlstedt, 2013).

The common denominator of the three abuse mechanisms is a continuous, uncontrollable increase in temperature within the battery, more commonly known as thermal runaway.

Thermal runaway may result in hazardous consequences, see for example GM Chevrolet Volt fire (Smith, 2012).

The purpose of the literature survey was to identify the main areas of concern regarding Li-ion battery safety, the primary source of the literature was Scopus (B.V, 2013) which is one of the largest databases for articles.

1.2.1 Brief introduction to Li-ion batteries

Li-ion batteries are composed of a layered structure in different configurations. The structure consists of anode (negative electrode during discharge), cathode (positive electrode during discharge), a separator (polymer film which separates the two electrodes) and current collectors on both sides of the electrodes (Sahraei, Hill, & Wierzbicki, 2012).

The anode material is usually composed of a layered carbon structure namely graphite. The cathode material is commonly composed of different types of lithium transition metal oxides (Sehlstedt, 2013).

In order to provide the ability of ion transport between the electrodes, the separator and cavity in between the electrodes are filled with electrolyte. The electrolyte consists of a salt (i.e. $LiPF_6$) typically dissolved in organic alkyl carbonate solvent (Sehlstedt, 2013).

There are three main types of casings used to contain the electrochemically active material of a battery cell:

- Laminated cell
- Prismatic cell
- Cylindrical cell

The laminated cell is created from polymer- and aluminum foils layered in sandwich structure. The battery's active materials are layered within the cell and stacked on each other. Prismatic cells have a similar shape but with the difference of a thicker shell, made from either polymer or metal materials. Cylindrical cells are usually created from sheet metal to form a cylinder, in this configuration the battery layers are wound to form a spiral (Axeon, 2012). Figure 1 depicts the graphical representation of the three battery types.

Figure 1, displays the three battery cell types. From left to right: Prismatic, Cylindrical and Laminated (Axeon, 2012).

Furthermore, in this report there are three different levels of battery configurations. The first level is the one described above, i.e. cell level. When multiple cells are installed together, either in parallel or serial (depending on what voltage the manufacturer wants to achieve), they form a battery module. The final level is the battery pack level where multiple modules are connected in either series or parallel (Team, 2008).

1.2.2 Abuse Mechanisms

There are three major types of abuse conditions when considering battery risk analysis: thermal abuse, mechanical abuse and electrical abuse. Thermal abuse is typically external or internal heating of the battery cell. Mechanical abuse can be puncturing, pinching, mechanical shock or crushing the battery cell. Electrical abuse is short-circuiting or over-/undercharging of the battery cell. As can be seen in Figure 2 from "*Risk Analysis about hazards involved in critical failure of Li-ion battery systems*" by D. Sturk, the three abuse types have a strong connection, i.e. all three can result in thermal runaway. Thermal runaway is a failure condition occurring when the battery's constituent materials begin to decompose exothermally (i.e. decompose while generating heat) which subsequently catalyzes further decomposition and more heat to be generated until the battery is either cooled down, vents or burst into fire.
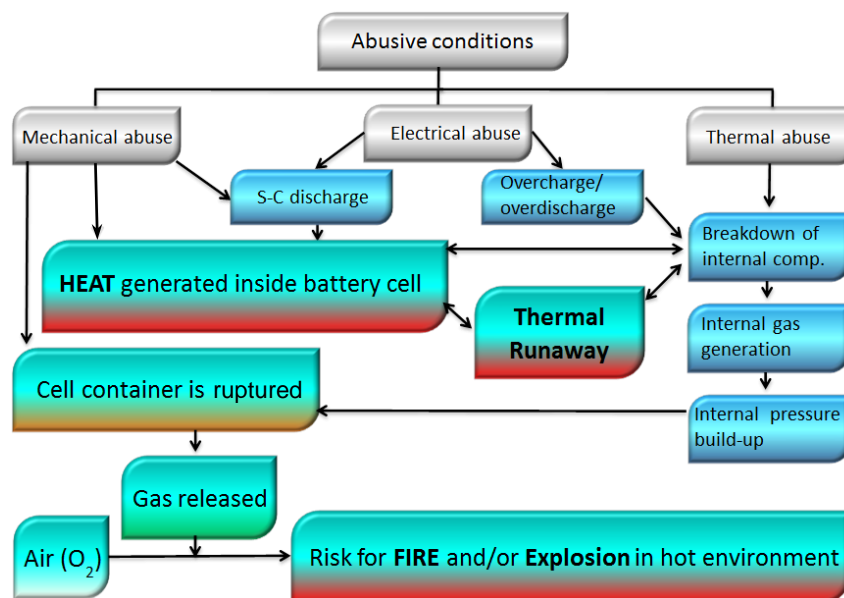
Figure 2, overview of how the three abusive conditions all may lead to thermal runaway and how the thermal runaway may result in critical failure (Sturk, 2012).

1.2.2.1 Thermal Abuse

When the battery experiences low temperatures, below its specified operational range depending on battery type and chemistry, the pore size of the Solid Electrolyte Interface (SEI) layer is lowered. This greatly reduces the transportation rate of Li-ions. If the battery cell were to be charged at this, lower than recommended temperature, the slow motion of the Li-ions through the SEI layer could result in lithium metal being built-up on the negative electrode, i.e. formation of dendrite needles across the separator. This could result in a cell internal short circuit from one electrode to the other across the separator (Ashish Arora, 2010).

According to Arora et.al. there are three reasons for battery cell failure at elevated temperatures (i.e. temperatures above the specified recommended operational temperature): SEI layer breakdown, electrolyte vaporization and state of charge (SOC) of the battery.

At high temperatures, approximately 120ºC, the SEI layer on the negative electrode (i.e. if using the common graphite based anode chemistry) starts to break down thereby exposing the electrode to the electrolyte. This may result in thermal runaway due to an exothermal reaction between the exposed negative electrode and the electrolyte (Ashish Arora, 2010). Those exothermal reactions will occur at a relatively low rate and the heat generated presents a relatively moderate power.

The second reason for cell failure is vaporization of the electrolyte. At elevated temperature the battery electrolyte will begin to evaporate at an increasing rate. This results in increased pressure inside the cell. When the pressure reaches the maximum threshold the cell casing can withstand, it bursts open through either dedicated pressure release vents or directly through the body of the casing itself. Subsequently the vaporized electrolyte will be exposed to ambient air. If a source of ignition is present or if the temperature is high enough (depending on battery composition) due to the cell's internal decomposition reactions, combustion in the oxygen in air is possible which results in massive amounts of heat energy being released, further worsening this thermal runaway condition due to aerobic combustion.

An increased SOC typically increases the magnitude of the consequences when experiencing abnormally high temperatures. High temperature in a charged cell increases the probability that the positive electrode will start to decompose while releasing free oxygen which then oxidizes the electrolyte exothermally. If the exothermic reaction is not hindered, the temperature can reach high enough to melt the separator, thereby causing internal short circuit and thermal runaway (Ashish Arora, 2010).

1.2.2.2 Mechanical Abuse

The main events that typically qualify as mechanical abuse are: mechanically shocking, crushing, penetrating and pinching the battery cell.

A mechanical shock originates from rapid acceleration of the battery pack. Mechanical shock can be experienced during collisions or due to dropping of the battery pack.

Crushing the battery could result in internal short circuit, due to contact between internal components, thereby causing a flow of current through the battery which has the potential to result in thermal runaway (Sahraei, Campbell, & Wierzbicki, 2012).

Penetration of the battery typically occurs by metal objects; polymers and softer materials typically break upon contact with the hard casing of the battery modules.

As a foreign metal enters the internal parts of a battery cell, short circuit may be initiated due to the metals conductivity itself and as well through self-contact of the battery's internal components. Nail penetration tests performed by Spotnitz and Franklin (Spotnitz & Franklin, 2003), presented in the report from Lisbona (Lisbona & Snee, 2011), indicate that shallow-depth penetration is more likely to result in thermal runaway than deep-depth penetration. This is due to the fact that a smaller contact area with the intruding material will limit the heat dissipated from the cell. Consequently, the temperature within the punctured cell increases more rapidly than if

a larger metal surface does intrude. Deeper punctures will correspondingly result in larger contact area and thereby higher heat dissipation from the cell to the intruding object, which will lower the heat build-up and thus reduce the risk of thermal runaway. The rate at which the puncture is penetrating the cell also influences the risk of thermal runaway. According to Spotnitz and Franklin (2003), low rate punctures resulted in temperatures as high as 600°C. High rate punctures deep inside the cell resulted in temperatures below 140°C (Lisbona & Snee, 2011).

1.2.2.3 Electrical Abuse

According to Lisbona and Snee (2011), the onset temperature for thermal runaway was 180°C for the undercharged battery cell in their test, but for an overcharged cell thermal runaway could be initiated at a temperature as low as 80°C. This shows that the SOC of a battery cell greatly affects the stability of the cell.

Lisbona and Snee (2011) also states that the rate of charging greatly affects the risk of thermal runaway; low C-rates does not result in thermal runaway whereas higher C-rates of about 9C typically does.

Internal and external short circuits are also classified as electrical abuse:

- External short circuit occurs when connecting a load with low resistance between the poles of the battery; consequently, a high flow of current is produced which greatly increases the temperature of the battery which may result in thermal runaway.
- Internal short circuit is typically a result of a conducting object entering the battery cell, thereby creating a high flow of current through the internals of the cell.

The high current in combination with poor heat dissipation from the cell to the surrounding environment typically results in high temperature increase. Maleki and Howard (2009) state that the location of the internal short circuit greatly affects the risk of thermal runaway. By having an internal short circuit deep inside the battery cell, the heat dissipation from the cell is limited and thereby the risk of thermal runaway increases due to the locally high temperature (Maleki & Howard, 2009).

1.2.3 Thermal runaway mechanisms

Described in the previous section, 1.2.2 Abuse Mechanisms, there are three main abuse mechanisms. These mechanisms are all likely to eventually lead to thermal runaway. Researcher E.P. Roth at Sandia National Labs, New Mexico US, has analyzed the thermal mechanisms of Li-Ion batteries with the following chemistries: NCA, NMC, Mangan Spinel and Iron Phosphate; and subdivided it into three parts based on cell temperature. Each one of these three stages is exothermal and generates heat due to reactions between the electrode components and the electrolyte.

1. The first stage is valid from room temperature until 150°C. This step is described as the onset of the thermal runaway. In this stage an anodic reaction with the electrolyte starts, resulting in a reduction of the electrolyte. At around 100°C the SEI layer on the anode starts to decompose, resulting in a relatively slow increased heat release. Although relatively slow, this heat generation causes further SEI layer decomposition to initiate at an increasing rate of reaction.

2. The second stage is valid from 150°C to 180°C. This step is described to be dominant of both venting, i.e. rupture of the cell, and additional acceleration in cell-internal heating. When the temperature reaches 150°C, an exothermic reaction starts to take place at the cathode material surface.

3. The third stage valid is from 180°C and above. At these temperatures the cathode material breaks down and results in a release of oxygen. The released oxygen further reacts exothermically with the electrolyte which rapidly increases the temperature of the cell. At this temperature the separator is likely to melt and thereby creating local short circuits. The short circuit result in joule heating of the cell (Ashish Arora, 2010) (Roth, 2008).

1.2.4 Thermal management

From the beginning of the market introduction of lithium-ion batteries in the 1990-ties (Shimotake, 1990) there has been much work carried out in order to enhance the overall safety. Critical for both overall safety and maximizing the battery system's lifetime is the Thermal Management System. This often critical system may be implemented both at cell- as well as in module level depending on vehicle manufacturer and the battery system manufacturer of their choice.

The main aim of the thermal management systems is to maximize the battery system's lifetime and minimize or hinder the risk of any critical conditions that may lead to thermal runaway and the consequences thereafter(Sehlstedt, 2013). The purpose of the thermal management systems present today is not to act during thermal runaway but rather act proactively to prevent battery failure.

There are two major types of thermal management systems being either Passive (Phase Change Materials or PCM) or Active (using air or liquid as coolant).

1.2.4.1 Phase change materials

PCM is usually composed of a paraffin wax dissolved into either a metal matrix or graphite. The metal and graphite structure is used to increase the latent heat of melting and to keep the structure intact during melting. Due to the matrix keeping the melting PCM in place the process is reversible, i.e. the material can undergo solidification to form its original shape by releasing heat energy.

Rao, Wang, and Zhang (2011) has conducted a study using PCM during operation conditions above normal, i.e. operation temperatures above that specified from the manufacturer as well as electric cycling with a higher than specified rate of change.

During both charging and discharging of the battery cells joule heat is generated. Due to the configuration of the cells within the module and also the property variations within the cells, there is a risk of great temperature variations over the cells.

The temperature variation between different cells should be kept below 5°C (Pesaran, 2002).

The concept of PCM is to use a material which starts to absorb thermal energy at the maximum operating temperature of the battery cells which is about 50°C depending on battery chemistry (Rao et al., 2011). This should keep the battery cells from exceeding its maximum operating temperature. Thermal energy is absorbed during the phase change of the paraffin wax from solid to liquid. By utilizing PCM this way, Rao et al. (2011) concluded that it is possible to lower the temperature variation between

the cells from 15°C to 5°C using PCM. The material also lowered the maximum temperature of the cells with 20°C. PCM has latent heat of melting varying from 200-255 kJ/kg (Rao & Wang, 2011).

Kizilel, Sabbah, Selman, and Al-Hallaj (2009) has conducted simulations of a battery module where one cell is subjected to abusive conditions, until being provoked into thermal runaway. Those simulations were conducted using twenty commercial 1.5Ah type 18650 cells. They conducted a comparison between air cooled battery cells and cells cooled passively using PCM. The aim of their study was to identify if PCM could prevent thermal runaway by distributing the heat generated from the faulty cell into the surrounding cells within the module.

Their simulations were based on an internal short-circuit where the faulty cells initial temperature were 170°C. In the air cooled model these conditions resulted in an increased temperature of the faulty cell pushing it into thermal runaway. The subsequent heat exposure onto the surrounding cells eventually resulted in failure and thermal runaway of all the cells within the module. Using the same criterion in the PCM model resulted in much faster thermal heat dissipation from the faulty cell to the PCM and the whole module. This is due to the intensive heat dissipation to the surrounding cells. The thermal runaway did not progress and the rest of the cells had a final temperature just above ambient.

Conclusions in the report from Kim, Gonder, Lustbader, and Pesaran (2008) states that PCM achieve its highest performance during short periods of high peak currents. When the PCM has absorbed a certain amount of heat energy, that amount of energy still needs to be evacuated somehow (e.g. forced cooling or by natural cooling). This would imply that using PCM as a last resort to avoid thermal runaway is not beneficial due to its inability to actually remove the heat energy from the system.

Furthermore, the report also states that PCM could potentially be used in vehicles using smaller batteries, i.e. batteries containing less energy. Using batteries which hold more energy, which potentially could transform into heat, the energy would be too much for the PCM to handle.(Kim et al., 2008)

1.2.4.2   Air Cooling

Air cooling of the battery pack is one of the simplest means in order to achieve an active thermal management system. Usually the air has a two-dimensional flow through the cross section of the battery module or battery pack.

Due to the low thermal conductivity and heat absorption of air, this system is limited to normal operational conditions of battery, i.e. it does not have the capability to mitigate critical thermal cell failure once initiated. The cell spacing within the module, i.e. the packaging, is a limitation of the amount of air flow which could pass through. (Rao & Wang, 2011)

In order not to restrict the cooling air flow through the battery pack, using air cooling requires more spacing between each cell/module inside the battery pack (depending on whether the manufacturer wants to cool on cell or module level). Conclusions from Pesaran (2001) states that using air cooling has lower complexity and weight but is less effective than liquid cooling. The need of relatively bulky flow channels in an air cooled battery results in a less compact configuration.

1.2.4.3 Liquid Cooling

In order to increase the thermal conductivity and the amount of energy which could be absorbed, liquid cooling can be utilized.

The heat transfer between the battery cells and the cooling medium can be carried out in several ways, e.g. by circulating the cooling medium inside piping/ heat sink which is in physical contact with the battery cell. Another way of achieving the same effect is to submerge the cells into dielectric fluid. (Rao & Wang, 2011)

According to Pesaran (2001), using liquid cooling is more complex and heavier than air cooling due to the increase in components and piping installation. However, liquid cooling offers higher performance compared to air cooling. Another benefit of using liquid cooling is that the installation is more compact compared to air cooling.

1.2.5 Battery Management System

In order for an active management system to maximize battery lifetime and minimize the risk of either electrical or thermal abuse there is a need for monitoring and controlling the individual cells within the battery pack. The main purposes of the Battery Management System (BMS) are as follows according to Lu, Han, Li, Hua, and Ouyang (2013):

- Monitor and control the voltage within a proper window of operation. This will hinder the risk of overcharging as well as undercharging i.e. maintaining a healthy battery over a long period of time.
- Monitor and control the temperature by utilizing the thermal management system. This will also increase the lifetime of the battery pack and minimize the risk of thermal runaway.
- Monitor and control the current flow both from and to the battery pack. This minimizes the risk of undesirably large joule heating of the cells.

1.3 Aim

The aim of this project was to:

- Evaluate potential failure conditions of vehicle Li-ion batteries through literature studies.
- Select a safety issue to which a safety product concept was to be defined.
- Investigate the required key components of this safety product concept.
- Conduct a preliminary validation of the product concept by simulations.
- Develop a test method and test rig for physical concept validation.
- Conduct physical testing of selected concept.
- Evaluate the selected concept's relevance to enhance battery safety.

1.4 Limitations

The project is conducted over a period of 20 weeks. The project does not aim to result in a final product but rather to investigate the selected safety concept in order to validate its potential relevance as a future battery safety product for E-Vehicles.

2   Method

Derived from the background study is the understanding that battery failure typically is a result of excessive heat generation in combination with poor heat dissipation. The solution to the problem in this report is to develop an emergency cooling system to reduce the temperature of the battery when an abnormal increase in temperature (which can be due to abuse or malfunction of the battery), above what is specified in the operating range of the battery, is identified.

The concept is to use a spray-on cooling system which will spray a liquid onto the surface of the faulty battery unit. The liquid should absorb the heat produced during battery failure and thereby reduce the risk of reaching initiation temperatures of thermal runaway by cooling the malfunctioning battery unit. Such action may also thermally shield off other neighboring battery units in case the malfunctioning unit is radiating heat.

2.1 Comparison between different Cooling Mediums

This section aims to give a brief comparison of the thermal properties between the spray-on cooling mediums considered for the simulations and physical tests that were carried out in this thesis.

In order to use a cooling medium as efficiently as possible, the medium need to undergo phase change. During phase change, a compound has the ability to absorb energy during constant temperature. Thereby, when using a medium at its melting or evaporation temperature, the medium will absorb energy without increasing its temperature.

Additional cooling efficiency can be achieved by pressurizing a coolant liquid and distribute it as a spray through a mist-generating nozzle. The coolant droplets will then be reduced in size as a consequence of the applied pressure and the design of the nozzle. In the case of water, in order to achieve high efficiency the droplet diameter should be equal to that of the wavelength of the heat radiation generated by the heat source to be cooled. Nonetheless, too small of a diameter will lower the droplets inertia and thus reduce its ability to travel throughout relatively longer distances or be distributed through narrow voids (Hertzberg, Hahne, Josefsson, Holmstedt, & Husted, 2004). Hence, an optimum droplet diameter should be aimed at in order to provide a liquid mist cooling system with as efficient cooling as well as distribution ability.

Moreover, when applying a cooling liquid the actual flow rate will affect the cooling power, and the duration of applying it will affect the cooling energy absorbed. Consequently, those two parameters must be taken into account as well.

2.1.1 Water as a Spray-on Cooling Medium

Using regular water as a spray-on cooling medium is beneficial when the temperature of the object to be cooled is above 100°C; this is due to the thermodynamic properties of water. At 100°C water undergoes phase change from liquid to gas form.

Temperature levels far above 100°C (e.g. above 300°C) are not relevant when considering an application to cool down an heated up Li-ion battery, since its temperature limit of thermal runaway cannot be considered as "far above" 100°C (see section 1.2.3 Thermal runaway mechanisms).

Nevertheless, since water does offer the ability to absorb large quantities of energy during evaporation (2260 kJ/kg during vaporization at 100°C and 1 bar) it presents good potential to act as a cooling medium about the temperature of vaporization.

2.1.2 Ammonia as a Spray-on Cooling Medium

Ammonia is commonly used as a refrigerant in large scale cooling systems, usually referred to as refrigerant R-717. It is a highly efficient cooling medium due to its thermodynamic properties. At atmospheric pressure, ammonia boils at -33.4°C (Products, 1999).

Anhydrous ammonia, i.e. pure ammonia, is irritating, flammable and colorless. It can cause eye-, skin- and respiratory burns. Inhalation is the most common way of exposure, typically resulting in irritation of the nose, throat and lungs. Overexposure may affect the central nervous system, typically resulting in unconsciousness and convulsions. 5 minutes exposure to 5000 ppm can result in death, which can be compared to oxygen composition in air which is about 210000 ppm (Shakhashiri, 2007). Autoignition point of anhydrous ammonia is 651°C. Ammonia combustion is typically extinguished by dry chemical, carbon dioxide or water. Ammonia leakage is easy to detect due to the strong odor which is recognizable at concentrations of 20 ppm (Products, 1999).

2.2 Choice of coolant

The idea used in this project is somewhat unorthodox. Initially, the idea was to expand compressed anhydrous ammonia through a nozzle, thereby creating a mist of cold ammonia gas which would cool the battery module. However, thorough research has proven that releasing high amounts of ammonia in air is dangerous as it will damage organic tissue. For this reason an alternative is to mix water and ammonia which will then be used to cool the faulty battery. Ammonia has good solubility in water, at 25°C 31% ammonia can be solved in water (ENGINEERING, 2004).

By mixing ammonia and water, a multi-step evaporation mixture is created. When the mixture is in contact with a heat source, the ammonia will evaporate before the water, thereby dissipating heat from the heat source. If the temperature of the heat source is above 100°C, the water will also reduce the temperature by its evaporation.

There are pros and cons of using this multi-step evaporation solution.

Pros:

1. It provides cooling at a lower temperature compared to conventional water spray cooling
2. It provides phase change at lower temperatures (e.g. evaporation of mixture starts at 25°C when using a mixture of 31% ammonia in water) compared to conventional water spray systems.
3. Its distinct odor provides an easy way to identify whether the system has been activated; this could be useful for rescue personnel.
4. Freezing point of a mixture of water plus ammonia is far lower than that of water, as can be seen in Figure 3.

Cons:

1. The toxicity of ammonia must not be neglected. When the ammonia evaporates from the mixture, pure ammonia gas will be released. The ammonia gas concentration in the passenger compartment must not reach above 300 ppm, which is the IDLH[1] limit determined by the NIOSH[2] (NIOSH, 1994).

2. A second drawback, based on the simulations carried out in this report, of using ammonia water mixture is the fact that it has a lower latent heat of evaporation. This means that these simulations indicate that the mixture does not have the possibility to absorb the same amount of energy as the pure water.

3. As mentioned above, pure ammonia gas may auto ignite although a sufficient external heat source (651°C) and correct mixture in air is required for ignition (Products, 1999).

The following graph (Figure 3) was obtained from ENGINEERING (2004), it shows the phase diagram of water-ammonia mixtures.
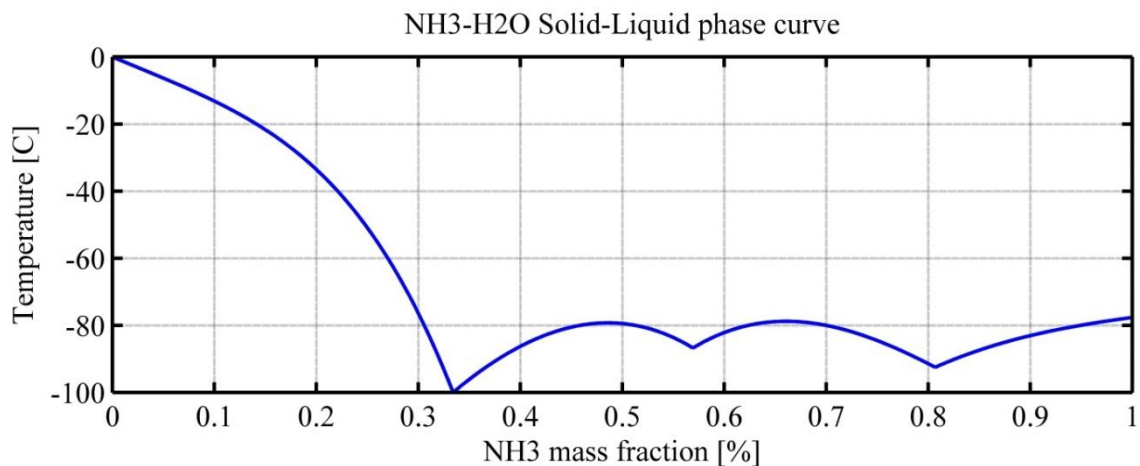

Figure 3, Phase diagram of water ammonia mixture.

As can be seen in Figure 3, when mixing 33% ammonia with 67% water, the mixture has a freezing point of -99°C. Considering a mixture of 25% ammonia and 75% water, the mixture has a freezing point of about -51°C.

2.3 Simulation of Thermal Properties

The potential energy absorption of a water-ammonia mixture was studied using the simulation program Aspen Plus V7.3. In order to identify the most suitable model for the simulation an evaluation of available calculation models was performed. By using literature studies in combination with guidance from prof. Lennart Vamling at Chalmers University of Technology, three different models were compared.

The three models are:

---

[1] *IDLH, Immediately Dangerous To Life of Health Concentration.*
[2] *NIOSH, The National Institute for Occupational Safety and Health.*

- Peng-Robinson (P)
- REFPROP (REFerence fluid PROPerties) (R)
- Electrolyte NRTL (Non-Random Two-Liquid) (E)

According to the guidance from L. Vamling as well as the literature studies, the REFPROP model was the model which resemblances reality closest when considering liquids (Aspen Technology, 2010).

Figure 4 shows the result of a simulated heating of 1 liter of 10% Ammonia-Water mixture from 20°C to 200°C when considering the three different models. The letters at the end of the legend name in the figure denotes the model to which it corresponds; E-Electrolyte NRTL, P-Peng-Robinson and R-REFPROP. As can be seen, the Peng-Robinson model differs quite a lot from the other two (displayed in Figure 4). There is only a slightly difference between REFPROP and Electrolyte NRTL models. As mentioned earlier REFPROP should be the model of choice.
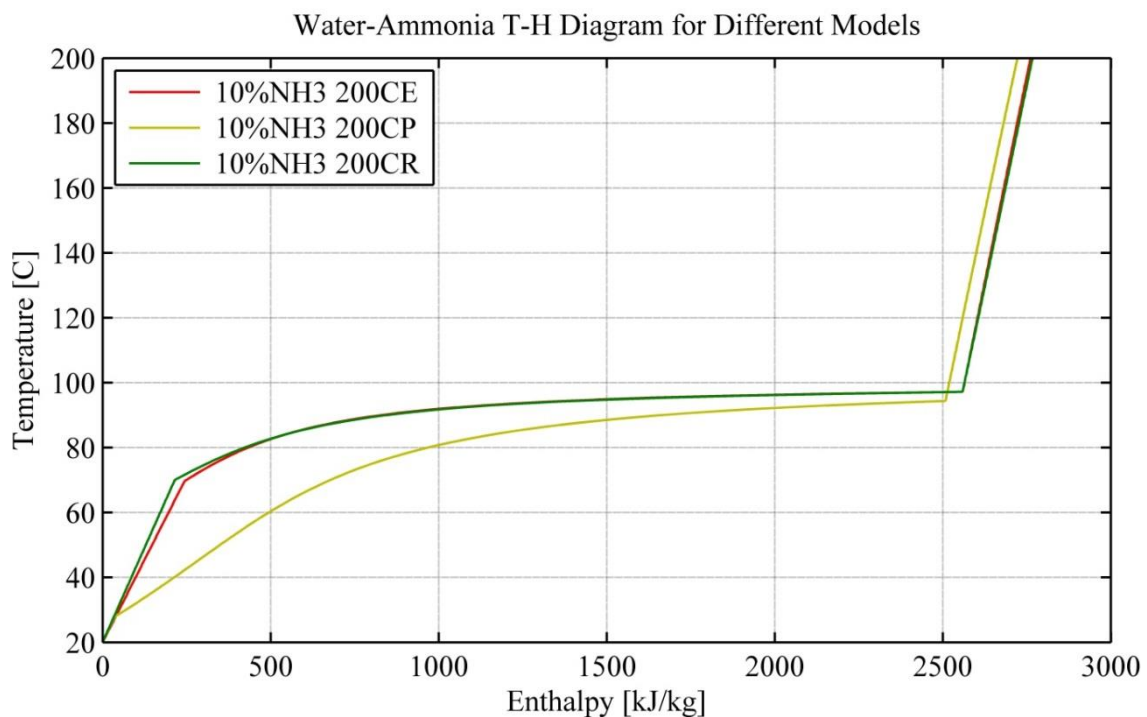

Figure 4, Enthalpy-Temperature diagram of Water-Ammonia mixture to compare behavior of the three models when considering 10%Ammonia-Water mixture.

However, troubles occurred when investigating the behavior of liquid compositions other than ammonia water using the REFPROP model. Therefore, the Electrolyte NRTL was chosen as the model of choice. The Peng-Robinson model was neglected as the simulated results differed from theory.

When the model of choice had been established to Electrolyte NRTL, the scenario was set up as follows to calculate the enthalpy of the mixture:

- Constant pressure at 1 atm.
- Closed-space container which does not allow any medium to escape (in order not to lose energy)
- The mixture is heated from 20°C to 200°C.

2.4 Experimental Setup

In order to verify and compare ammonia/water mixture cooling medium performance against other mediums an experimental setup is vital. The objectives with the test setup are:

- Calculate cooling power (i.e. the thermal energy per second which may be absorbed from another body) of different cooling mediums when sprayed onto a hot surface.
- Investigate the effect of spray nozzle design.

2.4.1 Estimation of the cooling power

One way to experimentally estimate cooling power is to derive the cooling power from a temperature profile retrieved from the object subjected to the cooling medium spray. Figure 5 displays the thermodynamic schematics of a system with known properties with which it is possible to derive the cooling power. The system boundary represents the object subjected to the cooling medium.
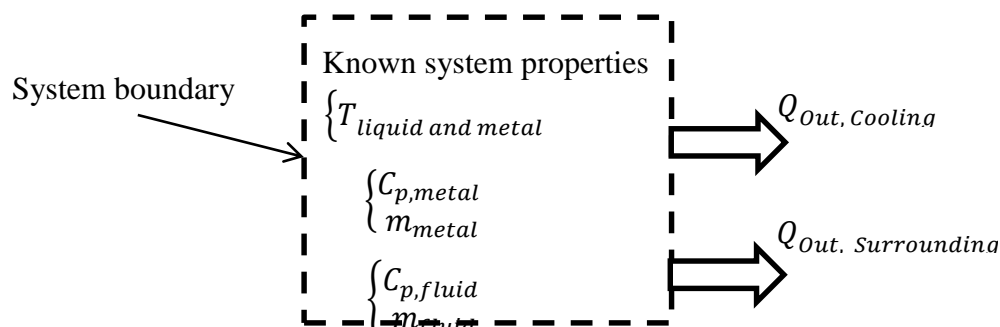

Figure 5, Displaying thermodynamic properties of the experimental setup

In order to make an appropriate estimation of the cooling power it is vital that the temperature profile of the system is known. There is an imminent risk of inaccurate temperature reading due to possible thermal variations throughout the interior of the tested object, which may arise from an uneven dissipation of heat to the surrounding, which could arise from uneven cooling of the surface. To minimize this risk it is desirable to utilize a fluid which can be circulated steadily and thereby equalize the temperature throughout the volume of that fluid. In order to prevent direct mixing of this fluid with the cooling liquid which is being sprayed onto a surface of the object to be cooled, the object needs to be a hermetically sealed canister. Hence, that canister will represent the system boundary illustrated in Figure 5.

Equation (2.1)-(2.3) displays the derivation of the system temperature on one hand, to cooling power on the other hand, based on known thermodynamic properties of the constituent materials of the warm object to be cooled. Equation (2.1) takes into account the heat dissipation to the surrounding.

Since the power calculation is a derivative value from the temperature profile, small oscillations with large gradients in the temperature profile will be reflected as high power, this may yield a result which is difficult to interpret. The temperature data as a function of time from the sensors is assumed to be similar to a function based on newton's law of cooling. Based on this hypothesis, a Gaussian function seemed to provide the exponential part of the equation. However, the degree of the Gaussian function needs to be evaluated when all data is received. The results will be based on the Gaussian function (2.4). The actual fit of the Gaussian function will be discussed further in the Results section 0.

$$\Delta U_{system} = (C_{p,fluid} * m_{fluid} + C_{p,material} * m_{material}) * \Delta T_{fluid\ and\ material}$$ (2.1)

$$Q_{Out,Cooling} = \Delta U_{system} - Q_{Out,Surrounding}$$ (2.2)

$$P_{Out,Cooling} = Q_{out,Cooling}/\Delta t$$ (2.3)

$$f(x) = \sum_{i=1}^{n} a_i \cdot e^{-\frac{(x-b_i)^2}{c_i^2}} \ ; where\ n\ is\ the\ degree\ of\ the\ Gaussian\ function.$$ (2.4)

2.4.2 Prototype

The following sections describe the different parts of the test prototype.

2.4.2.1 Heat Storage Unit

Based on the previous assumptions, i.e. the theoretical model, a practical test rig design of the object which is subjected to the spray-on medium was developed. Figure 6 displays the prototype of the canister – from now on referred to as Heat Storage Unit (HSU) – and its ingoing parts which will collect the temperature readings.

The HSU is made of aluminum due to the high thermal conductivity properties and is sealed using a lid with a screw joint. Its high thermal conductivity will contribute to a uniform heat distribution throughout its cross-section. The HSU is filled with heat transfer oil "Castrol Perfecto HT5". The oil has desired thermodynamic properties such as:

- Boiling point of 343°C which is above that of the desired operation temperature.
- Relatively high thermal conductivity.

("Castrol Perfecto HT5," 2009)

The oil is circulated throughout two pipes illustrated to the right in Figure 6. Described previously in section 2.4.1 is the fact that the liquid within the HSU needs to be circulated, which is achieved by a pump located outside the HSU. The rotation is achieved by angle the inlet and outlet pipes.

In order to gain the appropriate initial temperature of the HSU a heater is used.

On top of the HSU a lid will be placed at which the cooling medium should be sprayed onto.

The temperature readings are collected from four different positions of the HSU illustrated with the colored circles in Figure 6.

Yellow circles indicate the position of the thermocouples submerged in the circulated oil. The thermocouples positioning is divided to give a temperature reading in the inlet as well as the outlet. Difference in temperature between inlet and outlet will indicate heat transfer between the system boundary and its surrounding.

Red circles indicate the position of the outside surface/lid mounted thermocouples. These thermocouples collect temperature readings from the surface at which the cooling medium is sprayed upon. The two sets of temperature measurements, i.e. submerged and surface mounted, will illustrate the overall cooling efficiency in terms of power and energy.
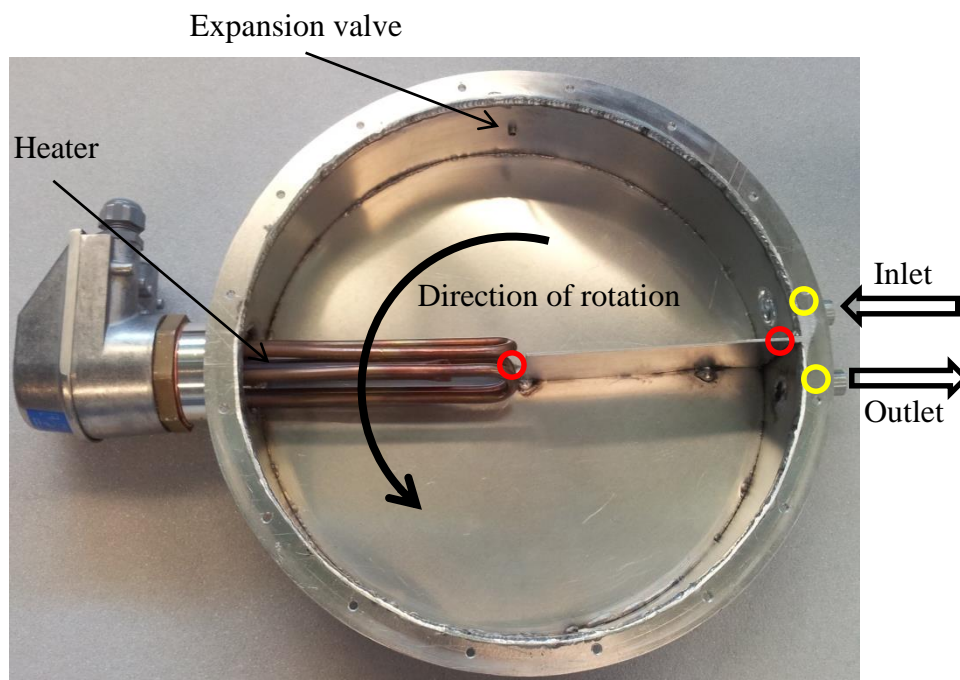

Figure 6, displaying the HSU and its ingoing parts which are subjected to the cooling medium spray. Yellow circles indicate the position of the thermocouples submerged in the circulated fluid. Red circles indicate the position of the surface mounted thermocouples.

2.4.2.2 Spray System

The objective of the spray system (i.e. spray nozzle, cooling medium container and propellant) is to deliver the liquid cooling medium in form of a spray mist. The flow rate, duration of flow and the droplet size is expected to affect the cooling characteristics and for that reason two different types of nozzles is tested using the same volume of liquid in all tests. The spray system for the experimental setup is illustrated in Figure 8.

The spray container, i.e. the device which holds the spray medium, has a circular cross-section and a moveable piston which is located inside this container. Furthermore, this piston divides the canister into two chambers. The first chamber contains the cooling medium while pressurized gas will be introduced to the second chamber. Consequently, the piston, and thereby the cooling medium, is propelled when pressurized gas enters the second chamber. On the outlet of the canister a changeable spray nozzle, depicted in Figure 7, is mounted. The cooling medium is thereby forced through the spray nozzle creating a spray mist. The nozzle hole diameter is the diameter which the spray liquid is forced through when passing the nozzle hole. A smaller nozzle hole diameter at a given pressure results in a reduced flow as well as a reduction in droplet size (BETE, 2013).
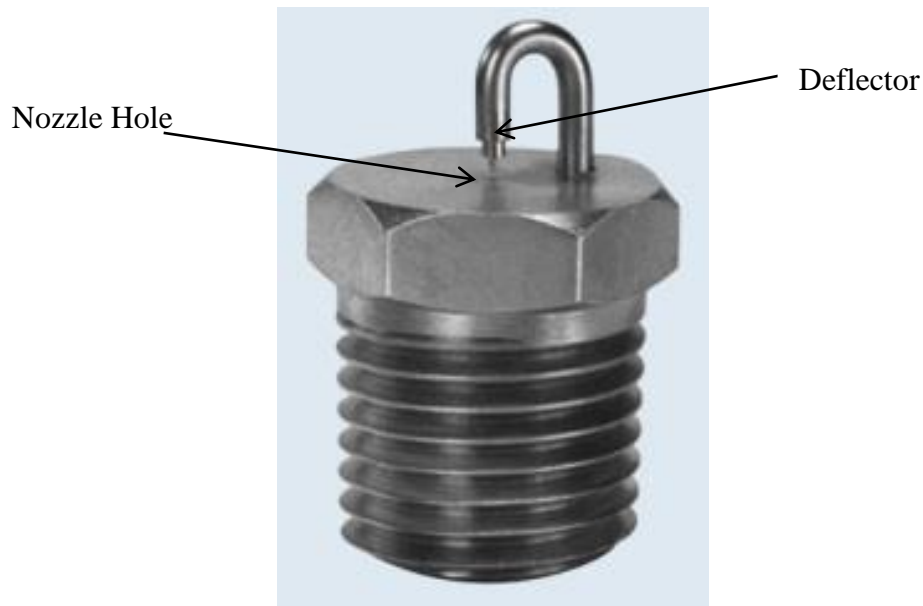

Figure 7, shows the PJ-series spray nozzle used in this project. Through the small nozzle hole, pressurized fluid is sprayed and the spray hits the deflector which separates the droplets to create an even finer mist and to define the angle of the spray cone (BETE, 2013).

The propellant, i.e. the pressurized air, is pressurized by using a commercially available compressor which delivers up to 13bar with a capacity of 100L of compressed air. Three important components are mounted in series between the compressor and the spray canister, i.e. a pressure regulator, manual valve, and an electric controlled solenoid valve. The pressure regulator gives the possibility of regulating the propelling pressure to the system. Regulating the pressure yields the possibility of controlling the coolant flow rate of the cooling medium as well as controlling the droplet size of the liquid.

The electric controlled solenoid valve gives the possibility of starting and stopping the system in a controlled manner.

The pressure reading is collected from two positions of the spray canister, one for propellant and one for the spray medium, their positions are indicated by the red circles in Figure 8.

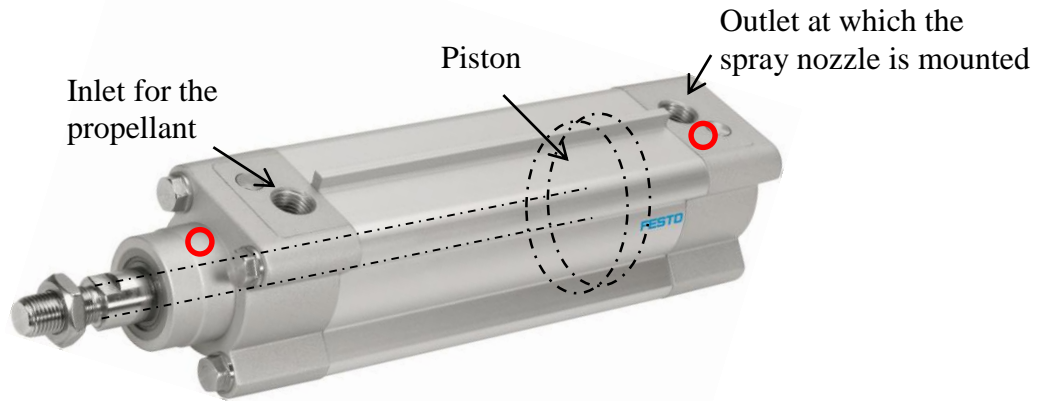The pressure gives an indication of start, stop and duration of the test.

Figure 8, displaying the spray container without spray nozzle. The black dashed line illustrates the insides of the cylinder, i.e. the piston and the rod. (Festo, 2013)

The main parts of the test rig described previously in section 2.4.2 are displayed in Figure 9 as an assembled unit. The spray nozzle, mounted to the spray canister, is placed directly underneath the HSU.

In order to minimize cooling medium contamination outside the test rig it has been sealed with polycarbonate plates.

Due to heat losses from the HSU to the environment it needs to be insulated to mitigate measuring errors. Proper insulation of the HSU is achieved by covering the top of the test rig with rock wool (not included in Figure 9).
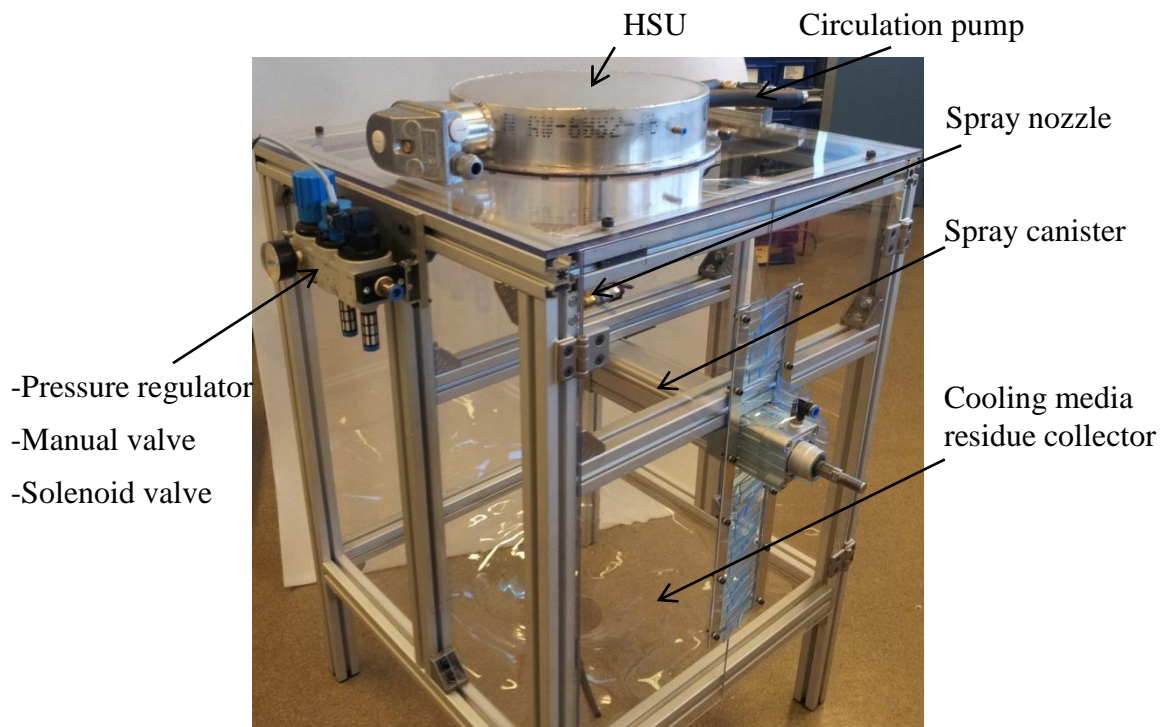

Figure 9, displaying the assembled test prototype without instrumentation and insulation

2.4.3 Calibration of the Test Equipment

This section describes the procedure of calibrating the sensors used during testing. It is crucial to have calibrated equipment in order to achieve reliable results.

2.4.3.1 Signal Collector

The test equipment's main signal collecting unit is used to collect the signals of all sensors and convert them from analog to digital so they may be processed in a computer.

The analog signals are stored in an onboard memory of the signal collector. When the test is finished, the analog signals are transferred to a computer.

The pressure and temperature sensors are connected to the signal collector, which in turn is connected to the test computer.

The sampling frequency of the signal collector was set to 100 Hz.

2.4.3.2 Test software

The program Crash Designer (Kistler, 2013) is used to configure test setups with the necessary sensors, i.e. pressure and temperature, and to handle the signals from the signal collecting unit. The runtime of the tests are also configured to match the duration of the coolant spray during each test.

2.4.3.3 Pressure Sensors

The pressure sensors from Kistler (Kistler, 2013) used during testing measures pressure difference from a given starting value. Before each test, the sensors were set to zero which means that once pressure is applied (i.e. when the spray system is activated) the pressure sensors will show the pressure difference (i.e. the relative value of the pressure).

2.4.3.4 Temperature Sensors

Thermocouples operate by using two different metals (conductors) coupled together. Upon heating the junction, the thermocouple will generate a voltage. The voltage will vary depending on the temperature of the metals. By measuring this voltage and using the so-called k-factor, with the unit μV/°C, the temperature of the thermocouple can be determined (Wikipedia, 2013).

The k-factor is determined by finding the value of how the voltage of the thermocouple varies over a given temperature range.

In order to calibrate the thermocouples, with the signal collector unit, used during the experiments, all four thermocouples were put in a heat chamber. By using a pre-calibrated temperature probe, the temperature of the oven was established for 5 different temperatures and the voltage of each of the thermocouples were noted. By using the values derived from the heat-chamber-test, the correct k-factor for each thermocouple was found.

2.4.4 Test Protocol

The aim of the tests is to compare the efficiency of the cooling medium over a wide range of temperatures, spray pressures and spray nozzles.

In order to achieve a good structure of the testing procedure a test protocol had to be established. By performing the same test two times the risk of coincidence was

reduced while still maintaining a reasonable time limit for the series of tests needed to be completed.

Three different starting temperatures were chosen for testing – 90°C, 120°C and 150°C.

The reasons for these three temperatures are:

1. 90°C to investigate whether ammonia/water mixture has higher cooling efficiency below the boiling temperature of water.
2. 120°C to evaluate how pure water performs above its boiling temperature compared to mixing it with ammonia.
3. 150°C to investigate the cooling efficiency of pure water and ammonia/water mixture at an extreme temperature, i.e. the lower limit temperature at which various Li-ion battery chemistries may start to experience an elevated risk for thermal runaway. This upper temperature is examined in order to evaluate if a spray-on cooling system can be used as a last resort at that lower limit temperature.

Two spray nozzles with different nozzle designs (i.e. generating two different droplet sizes) are used in order to evaluate how spray duration, flow rate and droplet size affects cooling efficiency. A design with smaller nozzle hole diameter at a given pressure and volume of cooling medium will result in elonger duration, lower flow rate and smaller droplet size and of the spray (BETE, 2013).

The ammonia/water mixture tests will be performed at 13 bars and then compared to the pure water tests at 13 bars.

The spray nozzle size and the pressure of the spray affects the time it takes for the spray medium canister to be drained. Therefore three different test runtimes were chosen. The larger nozzle will use a test runtime of 250 seconds regardless of the pressure. The smaller nozzle will use a test runtime of 400 seconds for the higher pressure, whereas 600 seconds will be required when using the lower pressure in combination with the smaller spray nozzle. It should be noted that the test rig does not need these durations just to be drained, the test times are rather chosen so that the signal collecting unit will receive excessive amounts of data and to make sure the signal collecting unit does not cut off in the middle of a spray test.

To make sure the temperature of the ammonia/water mixture and the pure water was the same, the mediums were placed together in separate jugs where the ambient temperature was 22°C. By doing this, any difference in temperature of the spray medium should not affect the difference in cooling rate significantly.

To achieve the best possible coverage of the spray mist on the HSU, a see-through polycarbonate plate was put on top of the test rig. The system was then activated and the spray showed a circular pattern on the polycarbonate plate. By measuring the diameter of the spray pattern, the height of the nozzle, in relation to the HSU, was adjusted to match the diameter of the HSU. This was done to minimize spray medium waste and assure best possible coverage of the HSU. See full test table in Table 5 in Appendix.

Prior to tests, the natural heat radiation from the HSU to the ambient air was determined. Even though the HSU is well isolated, there should be some heat radiation. To find this loss of energy the system was heated to the three individual test temperatures. The system was then left in this state, i.e. no additional energy was added nor actively removed, for 600s and the temperature of the HSU was logged. This provided the normal cooling curve of the HSU which was used to determine the heat radiation to the ambient air which was 22°C. Table 1 displays the resulting test matrix of stationary cooling.

Table 1 displays the test matrix to determine the heat radiation from the HSU to the ambient air when the test rig is at stationary conditions.

Test	Number of runs	Initial Temperature[C]	Cooling Time [s]
Test0C1	1/6	90	600
Test0C2	2/6	90	600
Test0C3	3/6	119,9	600
Test0C4	4/6	119,9	600
Test0C5	5/6	150	600
Test0C6	6/6	150	600

3 Results

3.1 Freezing point of Water/Ammonia mixture

The results of the theoretical freezing point of water/ammonia mixture are confirmed by placing a mixture of 25% ammonia and 75% water in a temperature chamber set to -43 °C. After nine days, the mixture was still liquid.

3.2 Enthalpy Simulation of mixture Ammonia-Water

From the simulation of heating a mixture of varying concentrations of ammonia and water from 20-200°C in a closed-space the result is depicted in Figure 10.

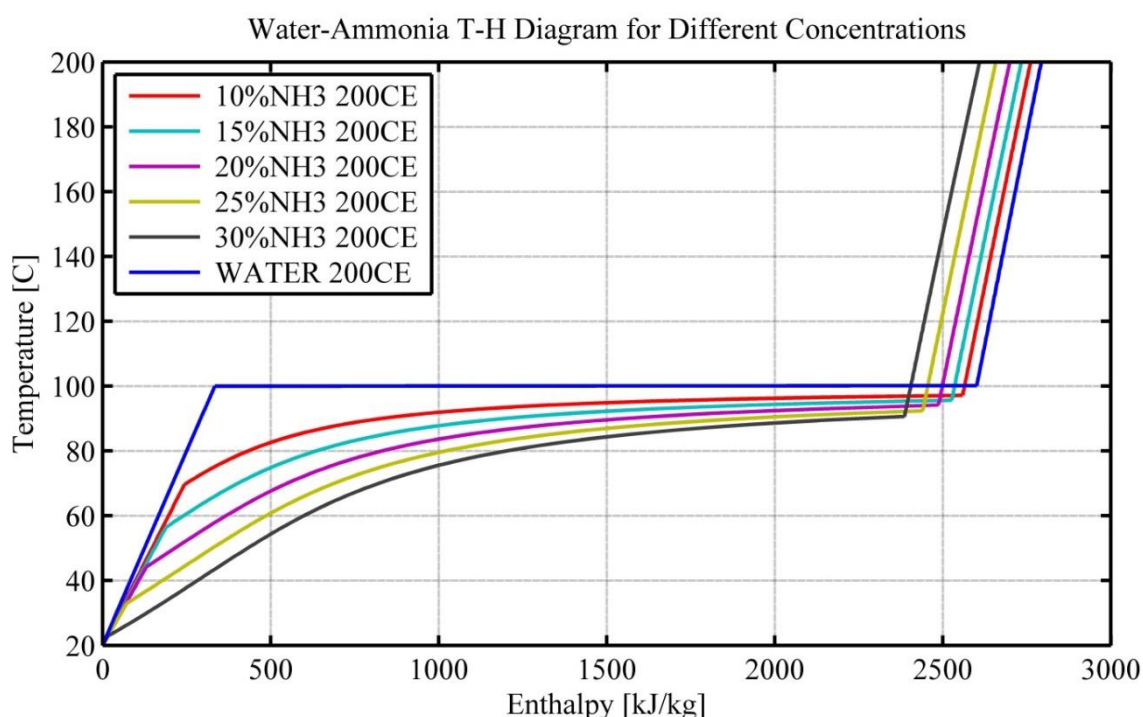**Figure 10, Enthalpy-Temperature diagram of Water-Ammonia mixture to compare the evaporation temperature of different mixtures of ammonia and water.**

Looking into Figure 10 and considering a mass of 1 kg mixture it can be seen that pure water absorbs approximately 334 kJ of heat energy before evaporation. Then, during an isotherm process the water can absorb an additional amount of heat energy of 2267 kJ. The result presented indicates that if a heat source with a temperature of 101°C is to be cooled with 1L of 20°C water, the water is able to absorb 2601 kJ.

As a contrast to pure water, the other curves in Figure 10, presenting Ammonia-Water mixtures, illustrates the fact that by adding ammonia to water the temperature of evaporation is lowered. Figure 10 also presents that the mixture's initiation of vaporization starts at a lower temperature, when more ammonia is mixed into water.

Studying the yellow curve of the aqueous mixture with 25% ammonia, the total amount of energy absorbed (2457 kJ) when increasing the temperature from 20°C to 101°C is less than the energy absorbed by pure water (i.e. 2601 kJ). However, the mixture's evaporation starts at a lower temperature which makes the addition of ammonia potentially beneficial in the event of aiming to supply cooling to a medium with temperatures below 100°C.

Another observation from Figure 10 is that simulation results show that the more ammonia added to the mixture, the lower the temperature of evaporation becomes; but on the other hand, the total energy absorption is reduced when comparing to water based cooling when starting at 20°C and up to 101°C.

3.3 Test Results

This section will present the results of the physical tests performed in the manner described in section 2.4.4. The graphs displayed will provide a possibility to compare both the cooling performance of a mist of water versus a mist of 25%Ammonia / 75%Water mixture when used as a spray-on cooling medium as well as what influence the size of the spray nozzle has on it.

Figure 11 depicts a generic result of the tests. It can be seen that the temperature on the surface of the HSU drops rapidly as the spray-on cooling is applied, whereas the temperature of the oil declines slowly. This particular graph is collected from test number 5 but the appearance is representative for all tests, i.e. the numbers, such as starting temperature and final temperature, between different tests are not the same but the appearance is. This figure is used only to show the behavior of the HSU when spray-on cooling is applied.
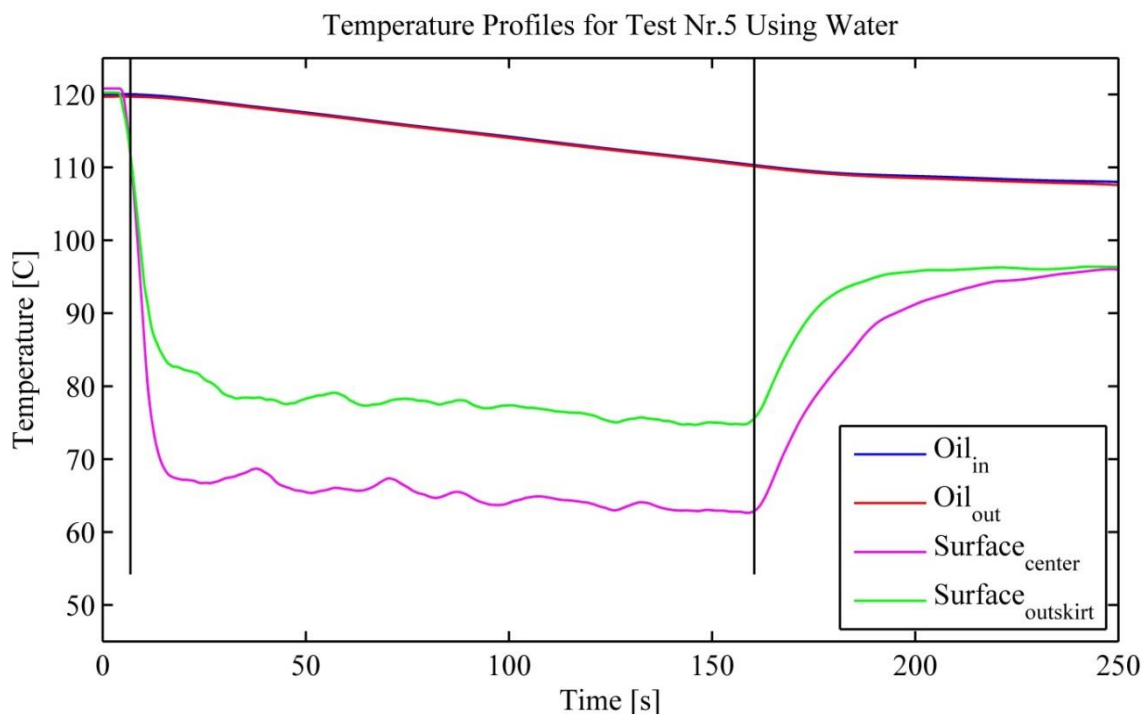

Figure 11, displays four different temperature profiles collected at different locations on the HSU. This result is from test number 5.

3.3.1 System Robustness

Figure 12 presents a comparison of the total cooling energy of two identical tests. As can be seen, the test system is consistent with high robustness when considering two tests.
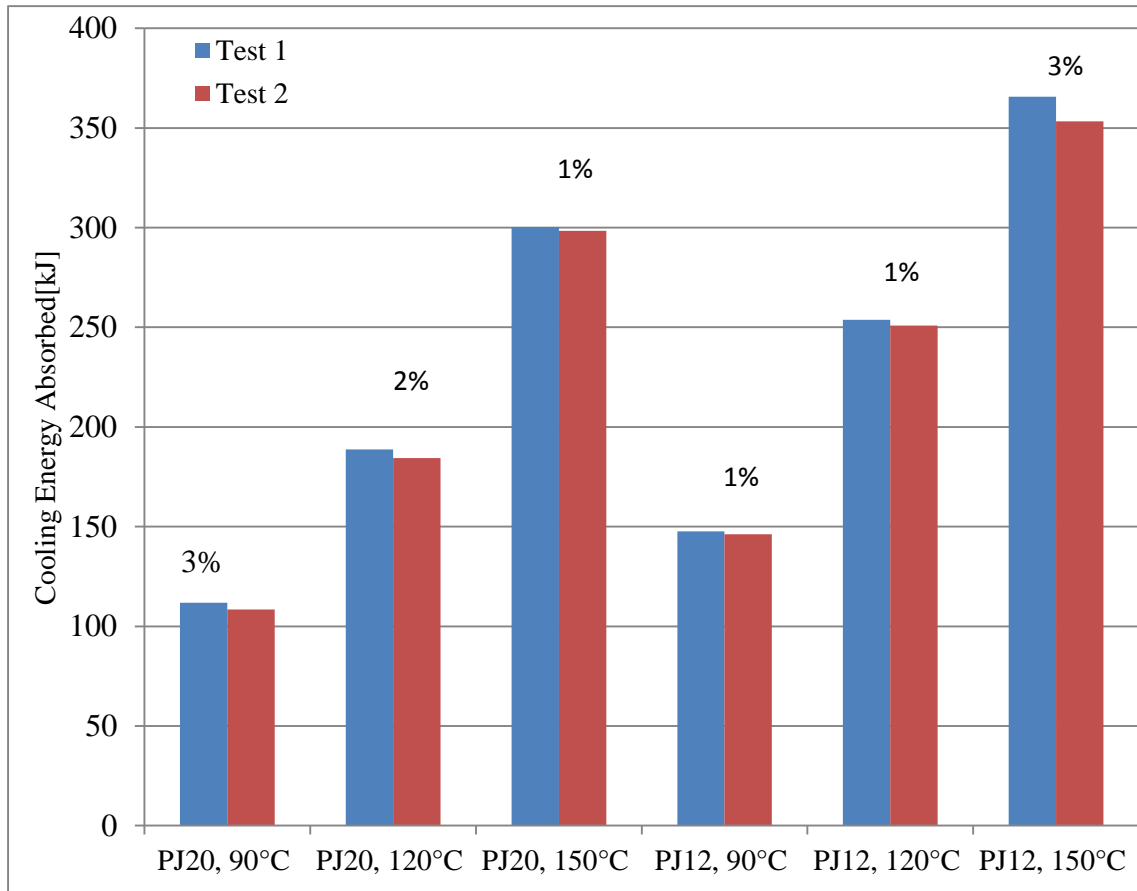

Figure 12, consistency test comparing total amount of cooling energy absorbed during tests. The percentage displayed above the bars are, the difference in total cooling energy between the two tests with the same specifications.

Figure 13 below depicts a comparison between the cooling power between two tests with the same specifications. This is another tool in order to investigate the robustness of the system. The cooling power is derived from the mean value of the cooling power during a time period of 50 seconds for the PJ20 nozzle and 150 seconds for the PJ12 nozzle. The duration is measured from 50 seconds after test initiation, which is chosen in order to avoid the fluctuations in the beginning of the test. The varied time duration is due to the fact that the flow rate of the nozzle with the smaller hole diameter is such that the flow duration is e approximately 300% longer.
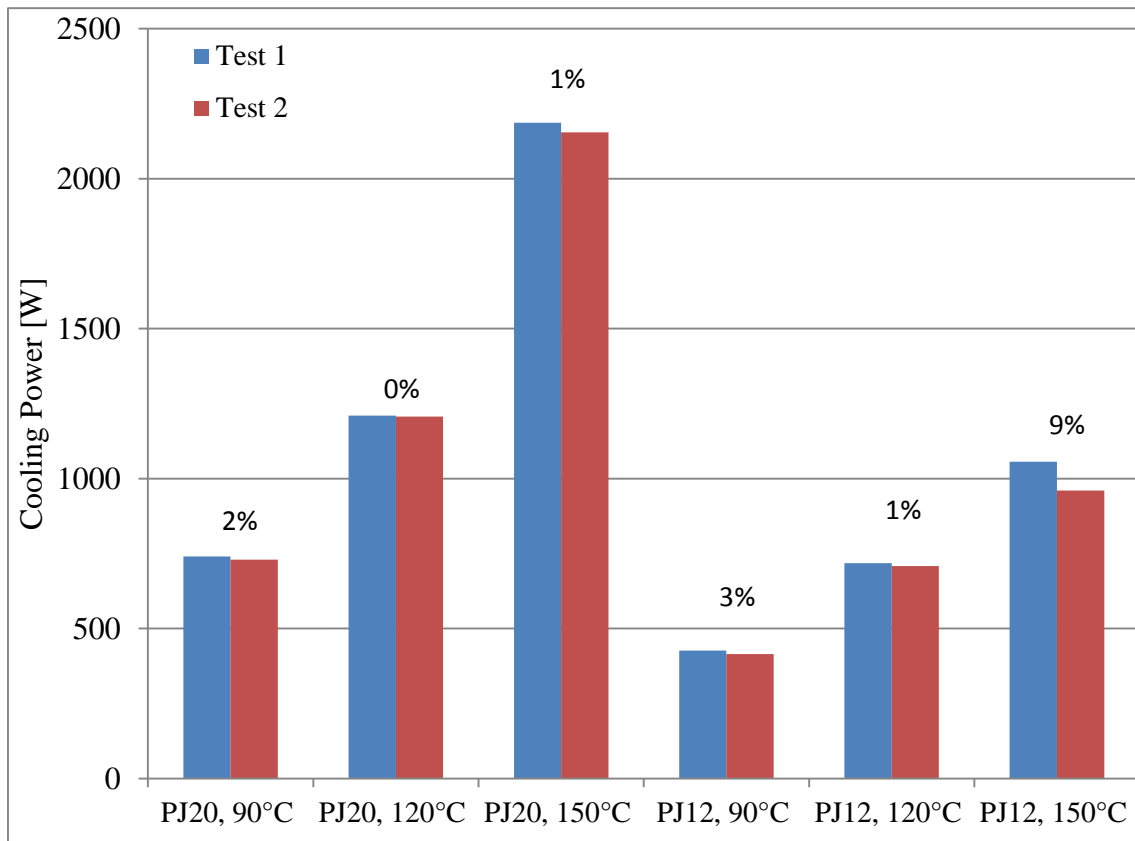
Figure 13, consistency test comparing total amount of cooling energy absorbed during tests. The percentage displayed above the bars are, the difference in mean cooling power during a duration of 50 seconds for the PJ20 nozzle and 150 seconds for the PJ12 nozzle between the two tests with the same specifications.

CHALMERS, *Applied Mechanics*, Master's Thesis 2013:

3.3.2 Curve fitting by Gaussian function

As described in 2.4.1 a 6th dimensional Gaussian function was used to approximate the oil temperature curve during cooling. As can be seen in Figure 14, the original data has a ladder shape, i.e. the data is close to constant during a relatively long period of time. The deviation of the 6th degree Gaussian from the original data is minimal.
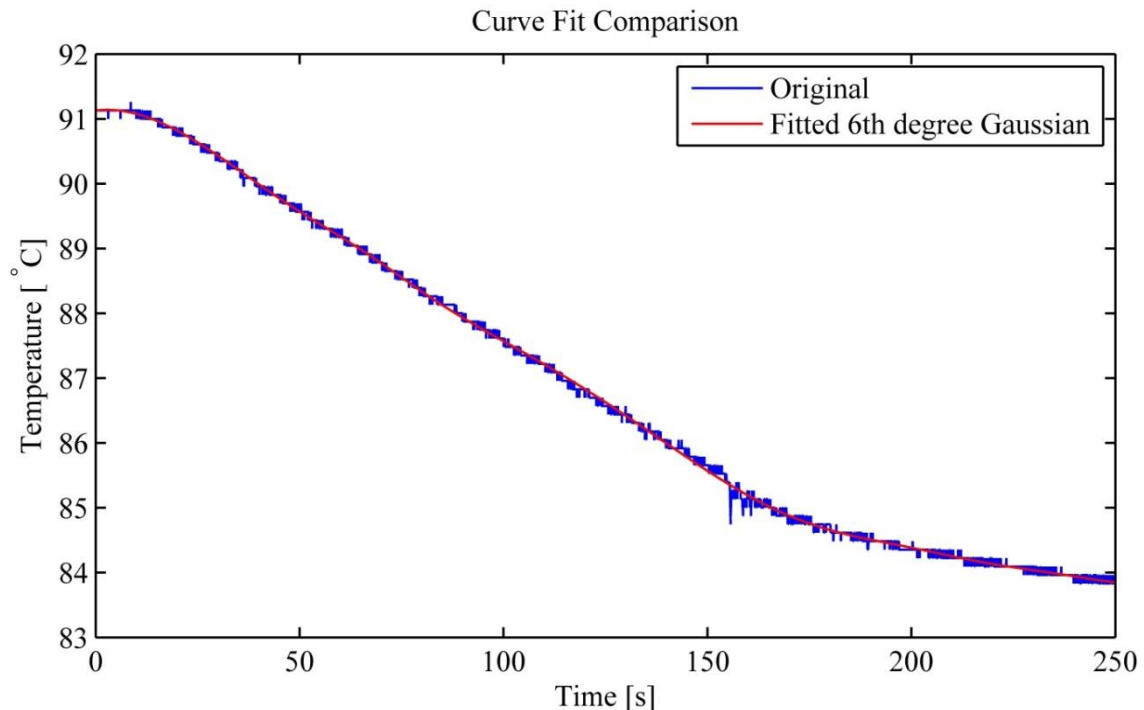

Figure 14, displays the original data with an overlaid 6th degree Gaussian function. The data is collected from test 1 and is representative for all tests as the appearance is the same except for absolute values.

3.3.3 Cooling Power Comparison between Water and 25%Ammonia / 75%Water Mixture

Figure 15-Figure 20 depicts the cooling power achieved using the two cooling mediums of interest. The first three plots presents the result of using nozzle PJ12, these are followed by three plots presenting the results of using nozzle PJ20.

Since PJ12 has a smaller nozzle hole diameter than PJ20 it has 294% longer spray duration (as can be seen by comparing any of the three first plots with either of the latter three), therefore the spray-time of PJ20 is shorter.
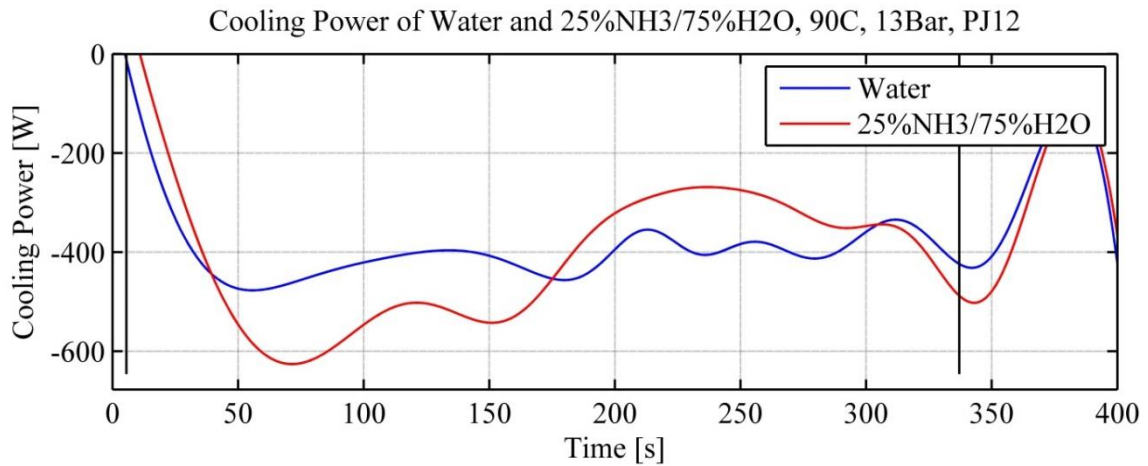
Figure 15, displaying the cooling power of water and 25% NH3/75% H2O. The Initial conditions of the test are; 90°C of the HSU, a spray pressure of 13Bar and the PJ12 spray nozzle. The black solid vertical lines, from left to right, correspond to start and end of the test respectively.

Figure 16, displaying the cooling power of water and 25% NH3/75% H2O. The Initial conditions of the test are; 120°C of the HSU, a spray pressure of 13Bar and the PJ12 spray nozzle. The black solid vertical lines, from left to right, correspond to start and end of the test respectively.

Figure 17, displaying the cooling power of water and 25% NH3/75% H2O. The Initial conditions of the test are; 150°C of the HSU, a spray pressure of 13Bar and the PJ12 spray nozzle. The black solid vertical lines, from left to right, correspond to start and end of the test respectively.
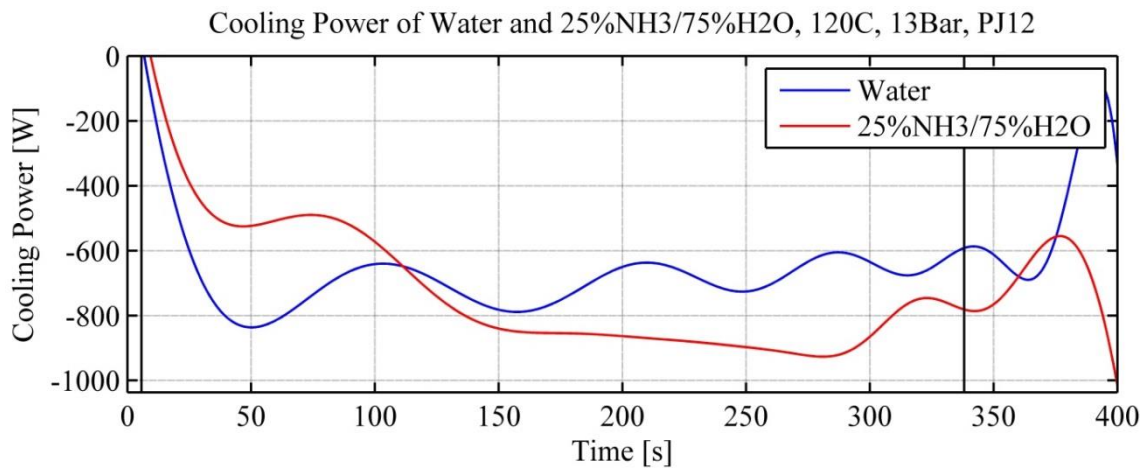
CHALMERS, *Applied Mechanics*, Master's Thesis 2013:
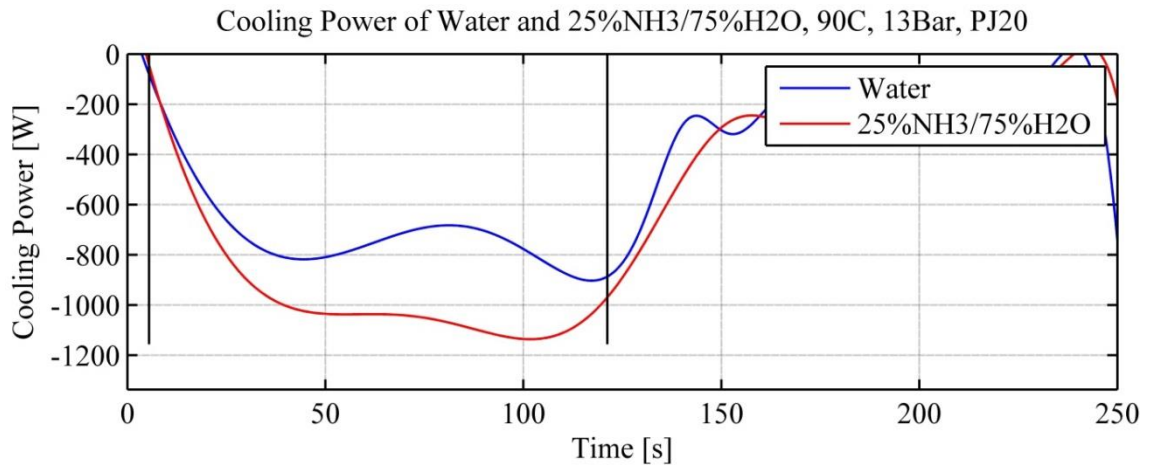
Figure 18, displaying the cooling power of water and 25% NH3/75% H2O. The Initial conditions of the test are; 90°C of the HSU, a spray pressure of 13Bar and the PJ20 spray nozzle. The black solid vertical lines, from left to right, correspond to start and end of the test respectively.
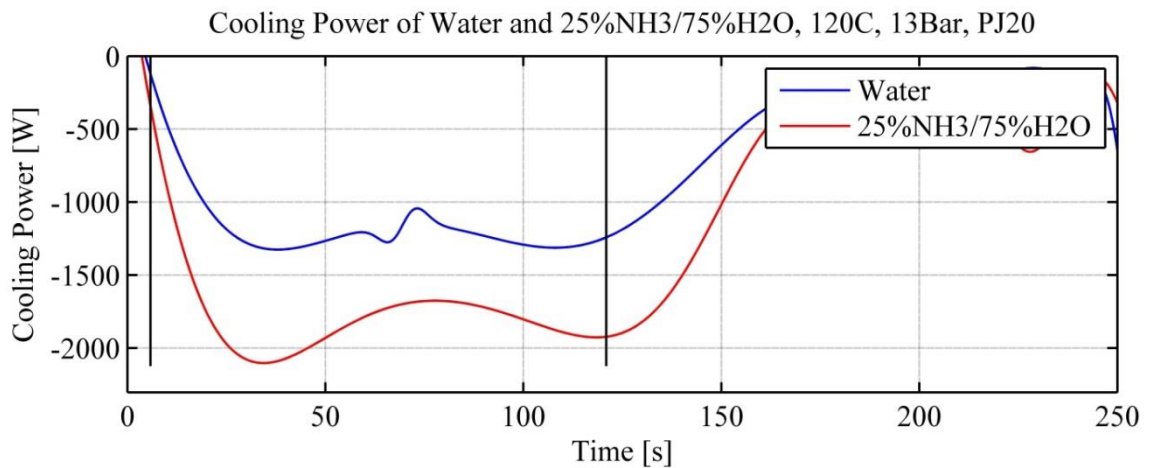
Figure 19, displaying the cooling power of water and 25% NH3/75% H2O. The Initial conditions of the test are; 120°C of the HSU, a spray pressure of 13Bar and the PJ20 spray nozzle. The black solid vertical lines, from left to right, correspond to start and end of the test respectively.
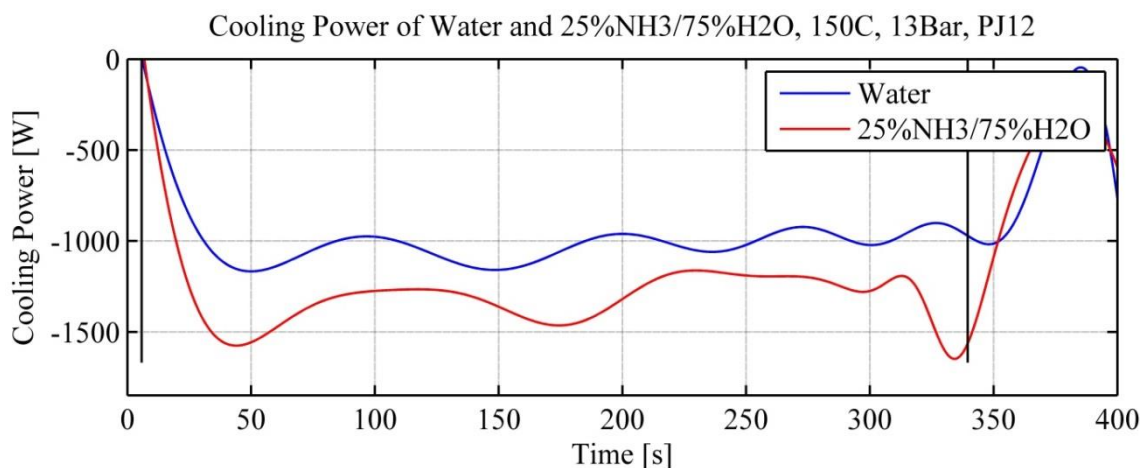

Figure 20, displaying the cooling power of water and 25% NH3/75% H2O. The Initial conditions of the test are; 150°C of the HSU, a spray pressure of 13Bar and the PJ20 spray nozzle. The black solid vertical lines, from left to right, correspond to start and end of the test respectively.
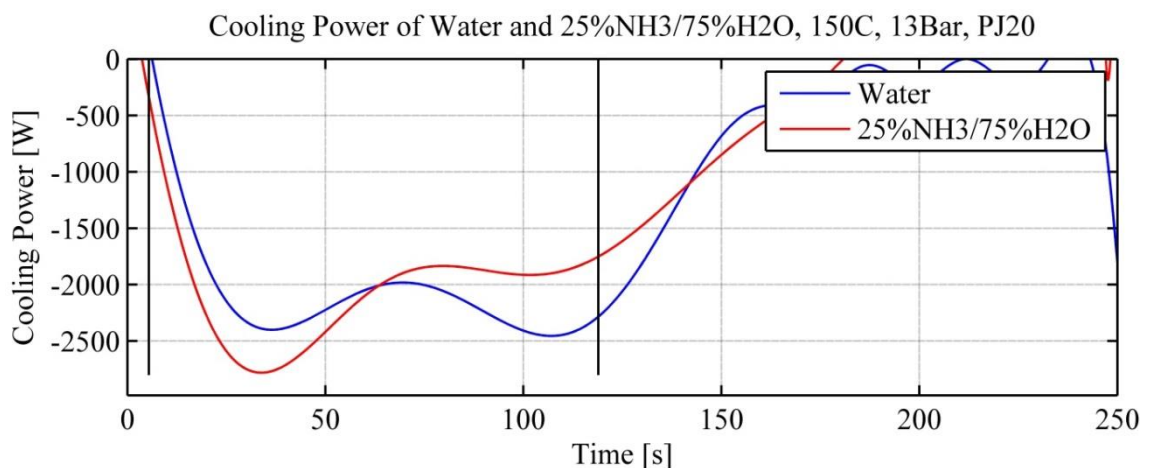
3.3.4 Surface Temperature of the HSU; Comparison between Water and 25%Ammonia / 75%Water Mixture

Figure 21-Figure 23 depicts the surface temperature of the HSU using the two cooling mediums of interest. The tests are categorized according to starting temperature of the test, i.e. 90,120 and 150°C. This makes it easier to visualize the lowest temperature which the HSU reaches during the spray test which is used to evaluate the performance of the spray mediums.

As can be seen in the following figures the surface temperature drops rapidly upon activation of the spray system. The temperature is then kept at an almost steady level apart from a slight declination. When the spray system is deactivated, the surface temperature of the HSU lid strives to reach the same temperature as the oil. Figure 21 is a typical example of where the sample duration was to short, i.e. the PJ12 test did not reach the temperature of the oil before the end of the test sample.

Figure 21, displaying the surface temperature of water and 25% NH3/75% H2O. The Initial conditions of the test are; 90°C of the HSU, a spray pressure of 13Bar. The two lines, named PJ20, are sampled with a shorter duration than those named PJ12. The sampling duration the PJ20 is 250s compared to PJ12 which has 400s.

CHALMERS, *Applied Mechanics*, Master's Thesis 2013:
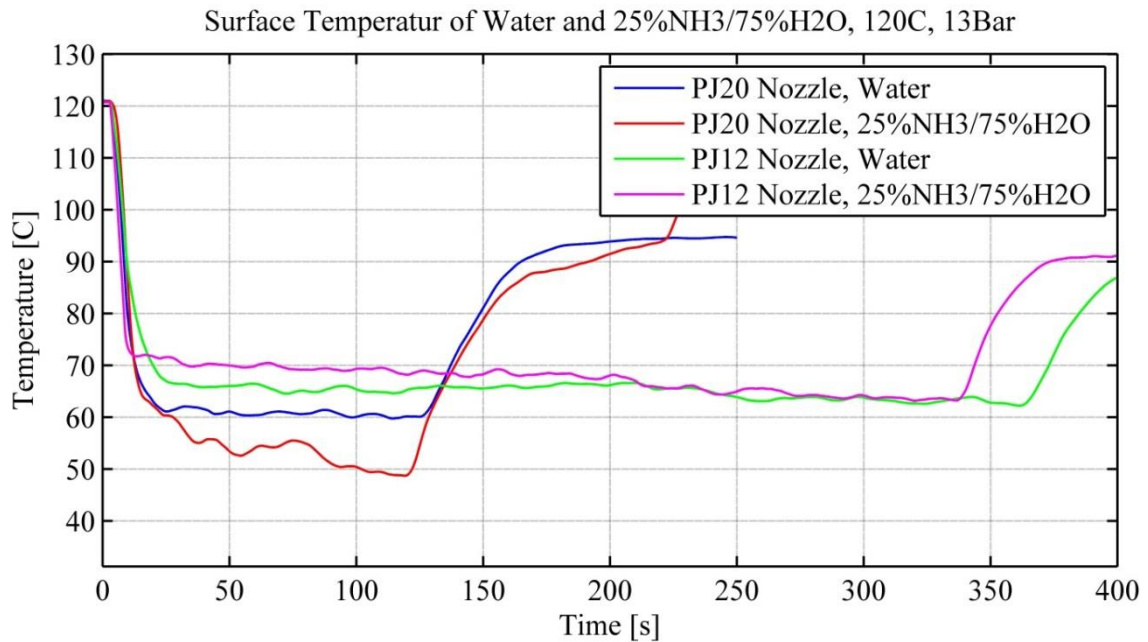
Figure 22, displaying the surface temperature of water and 25% NH3/75% H2O. The Initial conditions of the test are; 120°C of the HSU, a spray pressure of 13Bar. The two lines, named PJ20, are sampled with a shorter duration than those named PJ12. The sampling duration the PJ20 is 250s compared to PJ12 which has 400s.
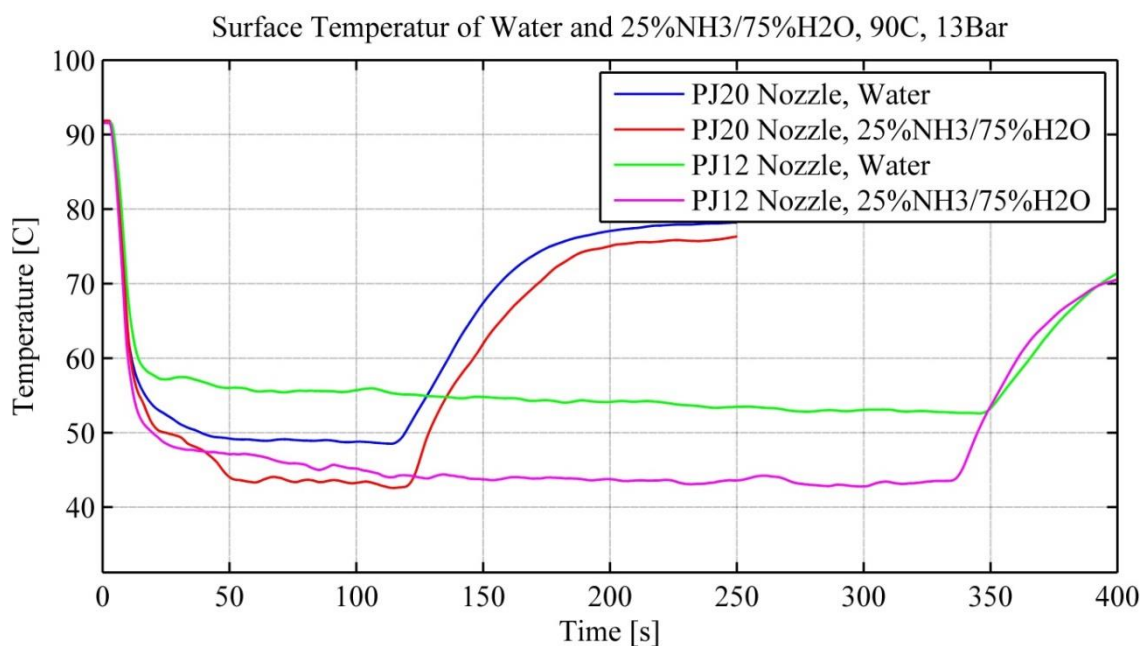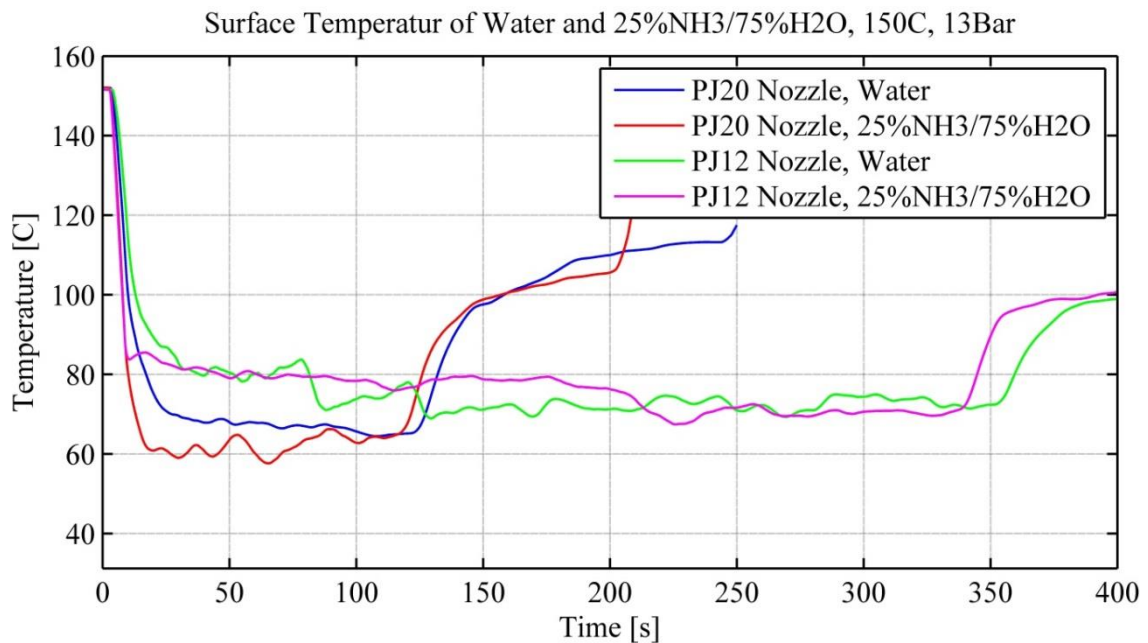

Figure 23, displaying the surface temperature of water and 25% NH3/75% H2O. The Initial conditions of the test are; 150°C of the HSU, a spray pressure of 13Bar. The two lines, named PJ20, are sampled with a shorter duration than those named PJ12. The sampling duration the PJ20 is 250s compared to PJ12 which has 400s.

3.3.5 Focusing on Initial Surface Temperature Drop

This section focuses on describing the initial stage after applying cooling medium to the HSU surface. Due to the low steady state temperature i.e. 50°C; 60°C; 70°C there are only partial evaporation during this sequence. Therefore in order to compare the cooling performance at evaporation temperatures, the initial sequence of the

temperature drop is in focus. Figure 24-Figure 26 below displays the temperature profiles of the two cooling mediums and the two nozzles during the initial sequence.
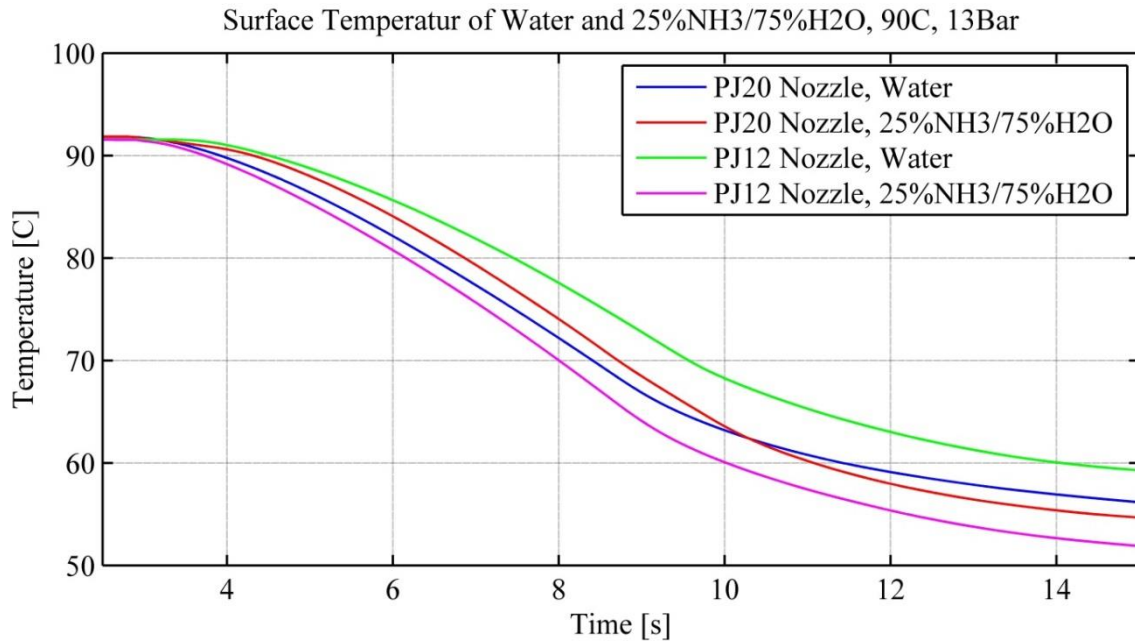
Figure 24, displaying the initial sequence of the HSU surface temperature. Two nozzles and two cooling mediums are compared. The initial temperature in these tests was 90°C.
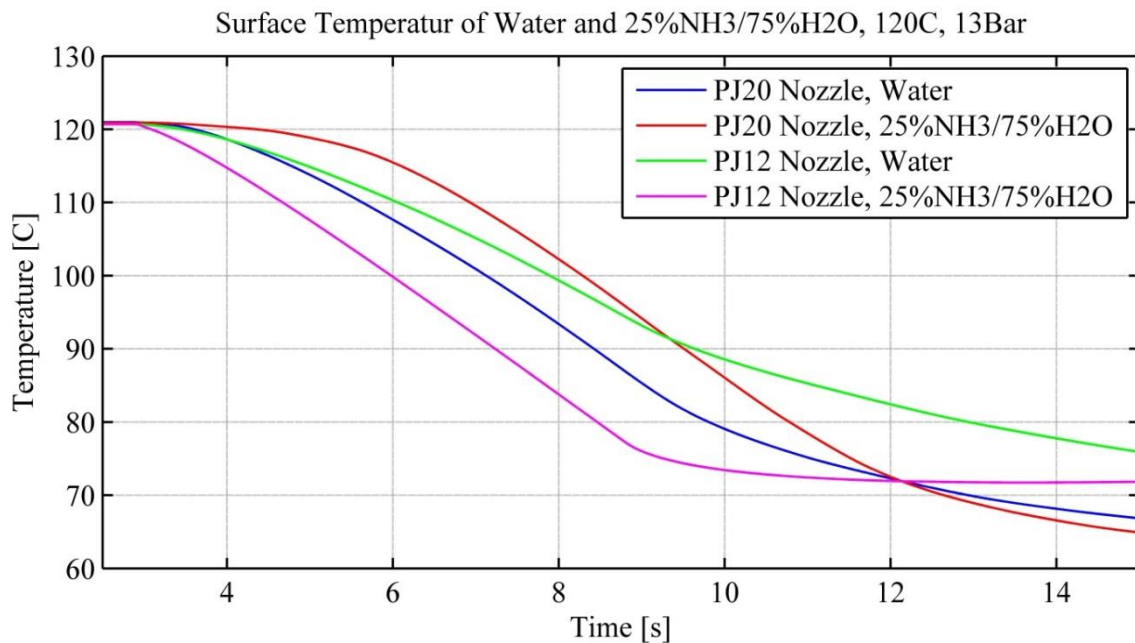
Figure 25, displaying the initial sequence of the HSU surface temperature. Two nozzles and two cooling mediums are compared. The initial temperature in these tests was 120°C.

CHALMERS, *Applied Mechanics*, Master's Thesis 2013:
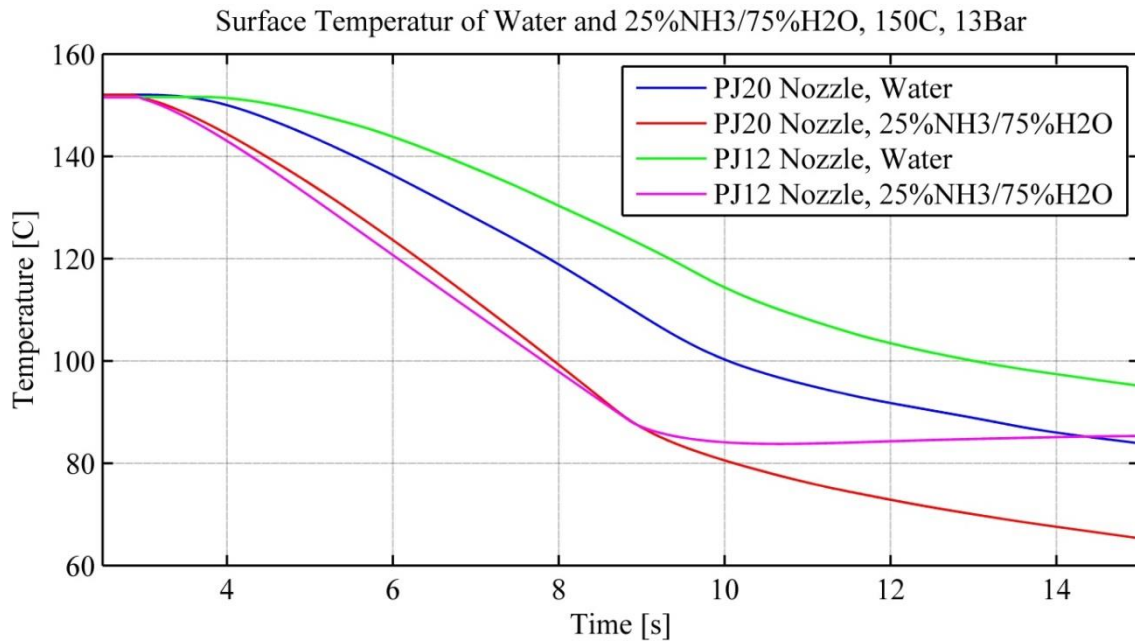
Figure 26, displaying the initial sequence of the HSU surface temperature. Two nozzles and two cooling mediums are compared. The initial temperature in these tests was 150°C.

3.3.6 Cooling Power of the HSU; Comparison between Nozzle Size and Cooling Medium

This section provides the results possible to compare the two different nozzle sizes. Figure 27-Figure 29 displays the cooling power for water and 25% NH3/75% H2O when comparing the two nozzles. The curves corresponding to PJ20 have different sample duration, therefore they are shorter.
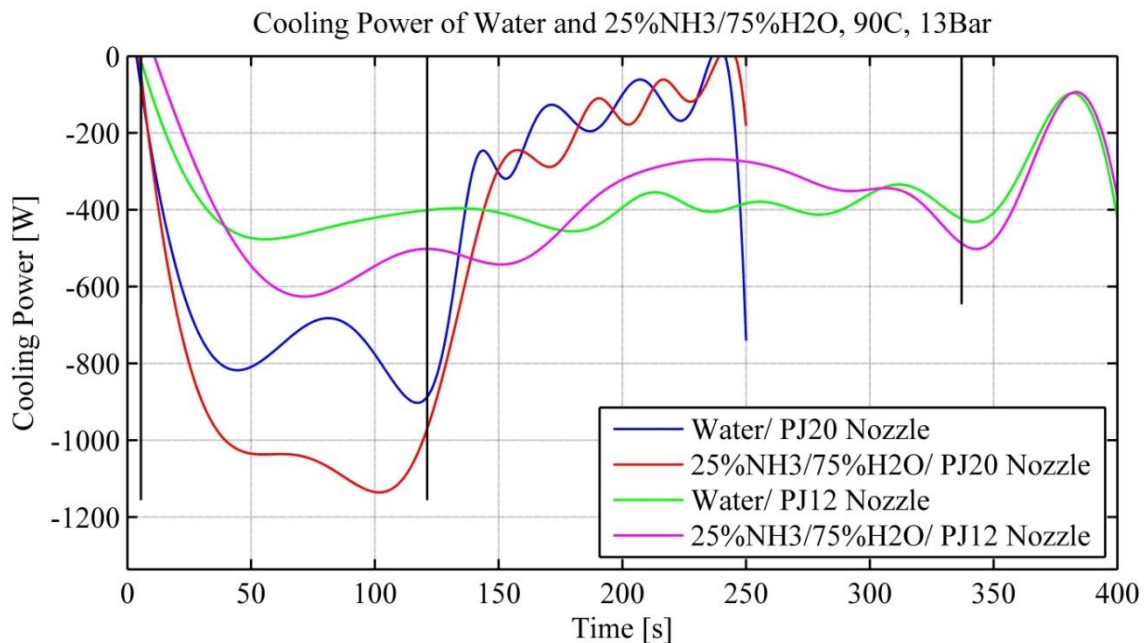
Figure 27, displaying the cooling power of water and 25% NH3/75% H2O using different nozzle size. The Initial conditions of the test are; 90°C of the HSU and a spray pressure of 13Bar. The black solid vertical lines, from left to right, correspond to start and end of the test respectively.

Cooling Power of Water and 25%NH3/75%H2O, 120C, 13Bar
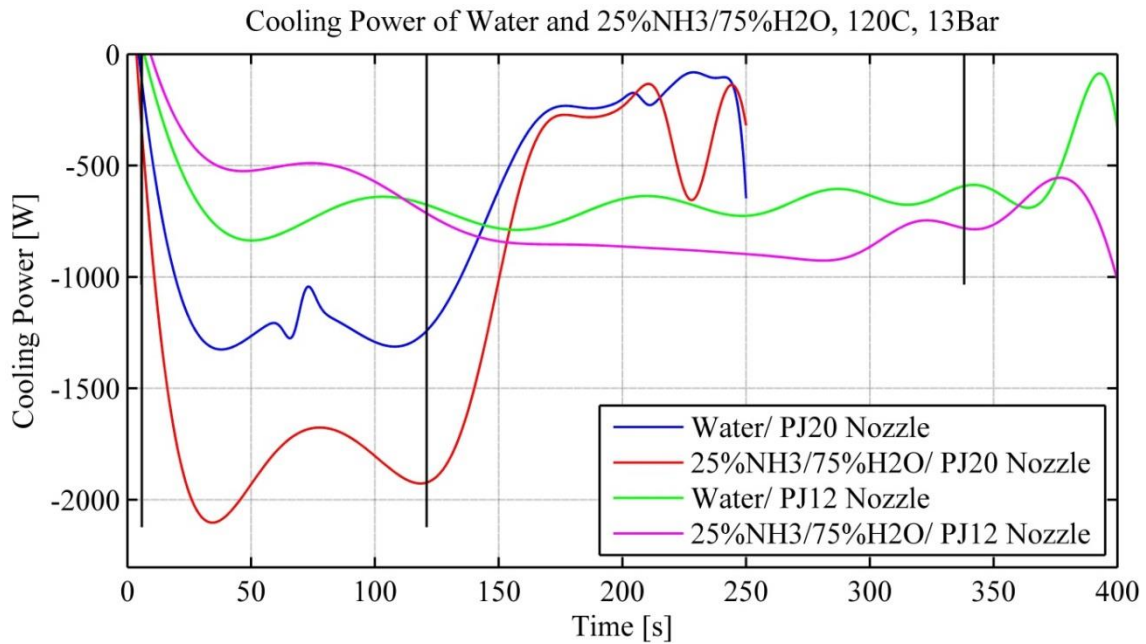
Figure 28, displaying the cooling power of water and 25% NH3/75% H2O using different nozzle size. The Initial conditions of the test are; 120°C of the HSU and a spray pressure of 13Bar. The black solid vertical lines, from left to right, correspond to start and end of the test respectively.

Cooling Power of Water and 25%NH3/75%H2O, 150C, 13Bar
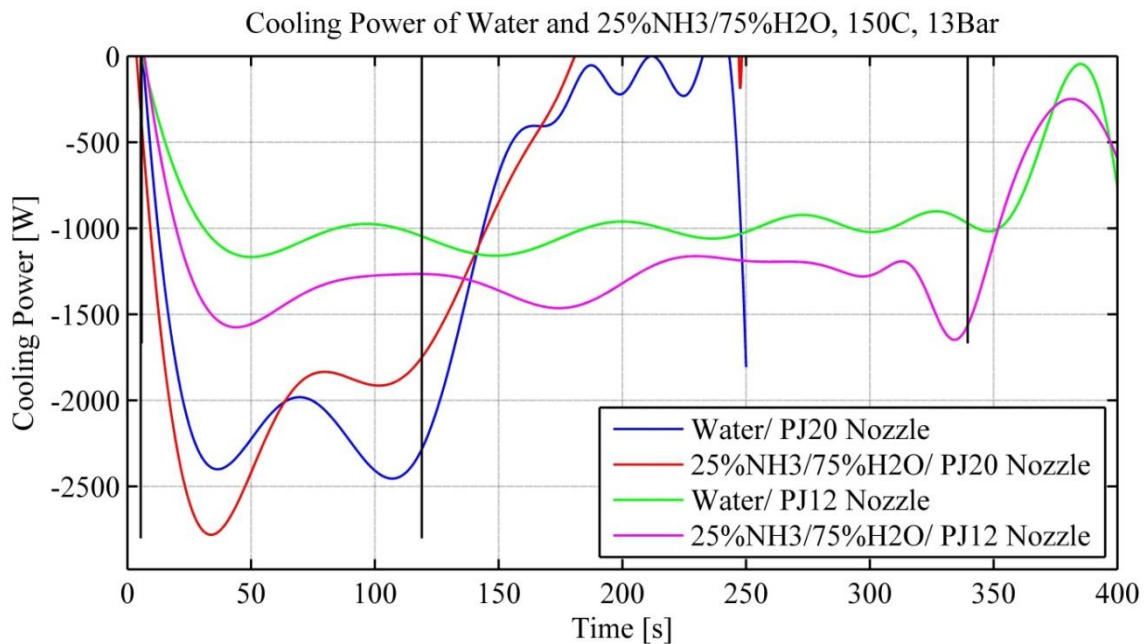
Figure 29, displaying the cooling power of water and 25% NH3/75% H2O using different nozzle size. The Initial conditions of the test are; 150°C of the HSU and a spray pressure of 13Bar. The black solid vertical lines, from left to right, correspond to start and end of the test respectively.

3.3.7 Total Heat Energy Transfer between the HSU and the Cooling Medium

Figure 30 and Figure 31 depicts the total heat energy dissipated away from the HSU. It also provides a comparison between the differences in cooling effects when using the two nozzles as well as between the two cooling mediums.

Figure 30 compares energy absorption increase when switching from water to 25% NH3/75% H2O.

CHALMERS, *Applied Mechanics*, Master's Thesis 2013:

Figure 31 compares energy absorption increase when switching from PJ12 to PJ20. The cooling energy presented in both tables is derived from the same collection of tests.
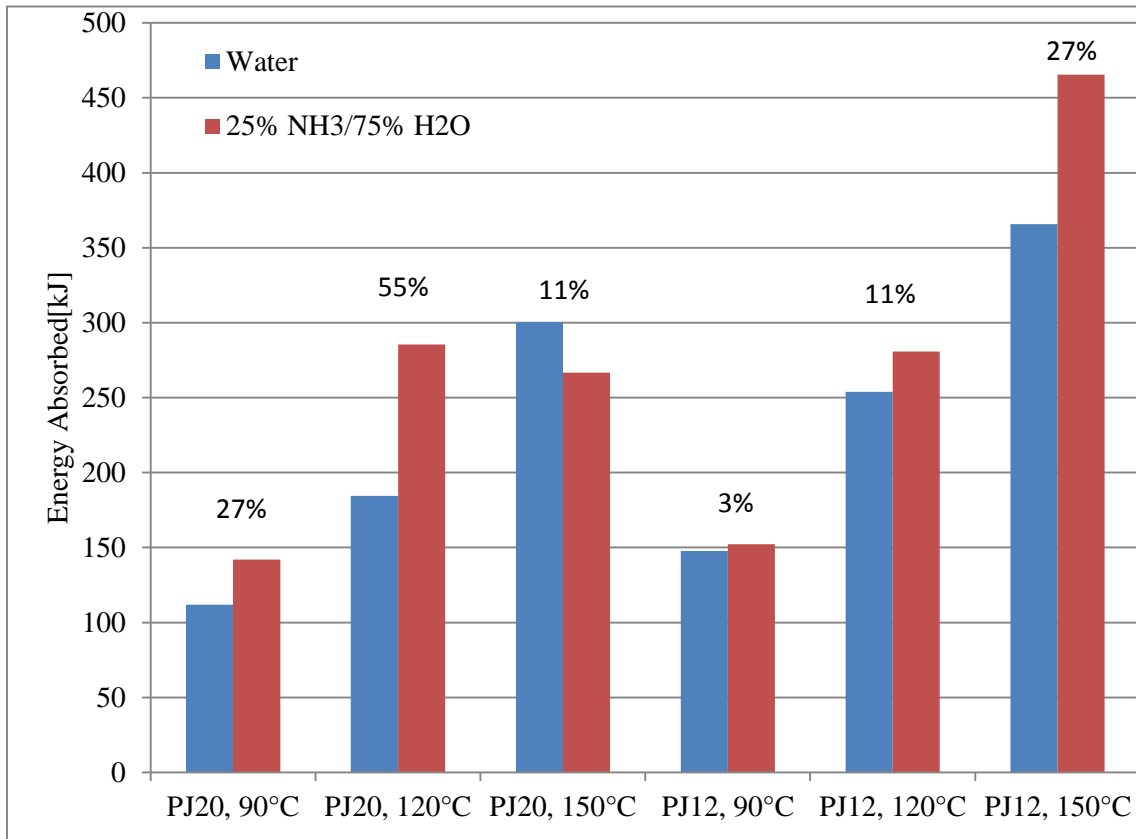
Figure 30, displays total energy absorbed using the specification specified at the bottom of each bar. The figure should be used to compare the two cooling mediums in terms of total cooling energy absorbed.
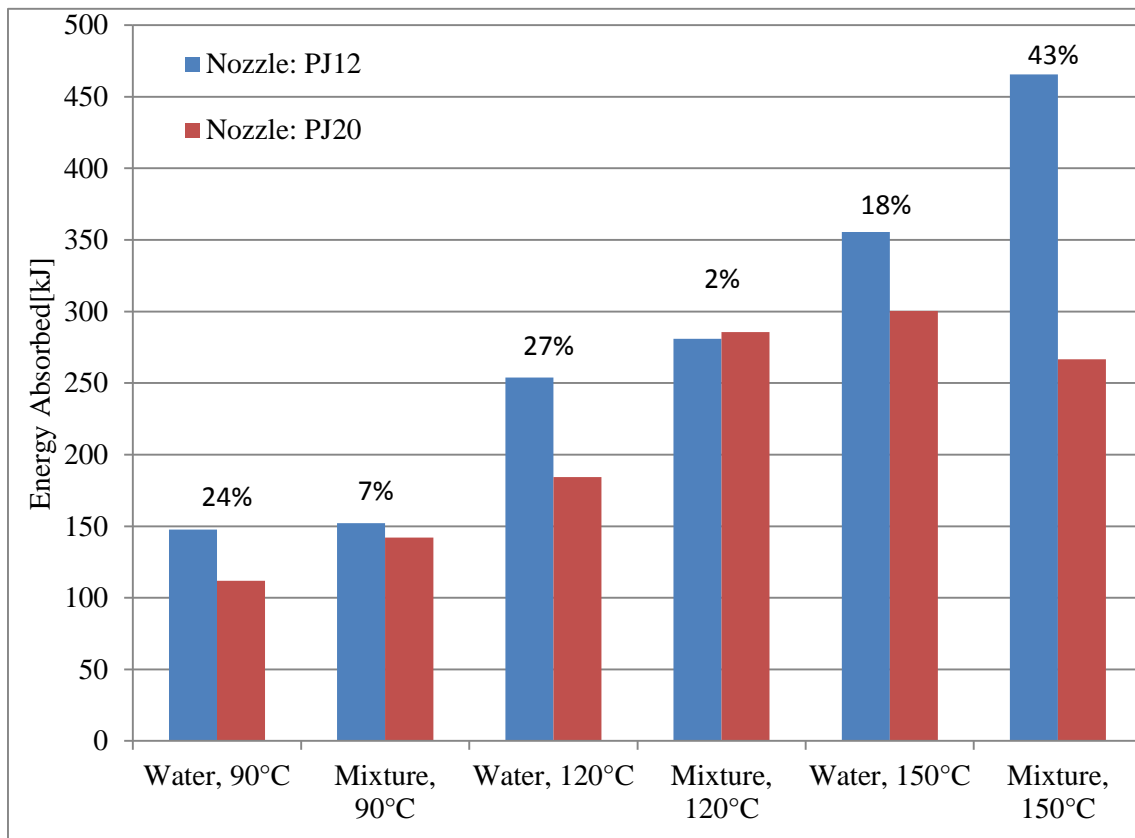
Figure 31, displays total energy absorbed using the specification specified at the bottom of each bar. The figure should be used to compare the two nozzles in terms of total cooling energy absorbed.

4 Discussion

Figure 12 show that the test rig has high consistency regarding total amount of cooling energy when two identical tests were compared. Similarly, Figure 13 shows that the cooling power between two identical tests was almost equal. However, in order to fully assess the consistency of the new test rig, additional tests should be carried out and data compared in terms of repeatability.

The experimental data show that spray-on cooling systems may be used to reduce the temperature of a surface and may in addition reduce heat radiation from a heat source to the surrounding, e.g. for use as thermal shielding of adjacent cells within a vehicle battery system. Both water spray and a mixture of 25% NH3/75% H2O rapidly cooled down the test surface that had an initial temperature of 90°C; 120°C; 150°C to a steady state temperature of approximately 50°C; 60°C; 70°C for water and approximately 45°C; 55°C; 60°C for 25% NH3/75% H2O.

After a rapid drop in temperature ending at approximately 15 seconds into the test, as depicted in Figure 11, the surface has reached an approximately constant temperature; thereafter only a slow and approximately linear temperature drop could be observed. This subsequent slow and linear temperature drop is a result of reduced heat transfer from the oil to the tests surface in the HSU as the temperature gradient between the applied coolant and the heat transfer surface in the test is lowered.

It was observed that the initial temperature of the surface to be cooled dropped rapidly from 90°C; 120°C; 150°C; down to approximately 50°C; 60°C; 70°C respectively, after about 5 s. This naturally results in a lower cooling power achieved than otherwise expected if the surface would have offered a steady state temperature at the level of the initial temperature, due to the lower temperature gradient between the cooling medium and the surface to be cooled. Consequently, in order to find the full potential of water as a spray-on cooling medium, the initial temperature of the HSU should be substantially higher in order for the surface not to drop below 100°C when the cooling is applied.

Figure 14 compares the 6th dimensional Gaussian function with the original temperature data. As can be seen, the original data has a ladder shape which would result in significant cooling power fluctuations. The fluctuation problem was solved by the representing the data with a Gaussian function. This function showed perfect correlation to the original temperature data.

The cooling power curves depicted in Figure 15-Figure 20 was derived from the oil temperature measurements. As a result of using the Gaussian function, the power curve is constrained to a number of criteria which the approximated curve holds. This may be reflected as the oscillations which has very low frequency (approximately 0,02Hz) in the power curve.

As can be seen in the end of some of the tests (e.g. Figure 16), the cooling power is not converging to zero; this is also a result of using the 6th dimensional Gaussian function. The approximated function has problems with minimizing the calculation error at start- and end point of the curves.

4.1 Comparing Nozzles

The results shown in Figure 27-Figure 29 indicates that in general the PJ20 nozzle increases the cooling power as compared to the PJ12. Figure 31 shows that using the PJ12 instead of the PJ20, generally yields a higher cooling energy, due to longer spray duration (i.e. 294% longer).

By comparing the energy absorbed by the cooling medium during the physical tests with the simulation results it can be seen that the spray on liquid is not fully evaporated. Investigating Figure 30 it can be seen that the total energy absorbed varies around 100-450 kJ/kg. Looking into Figure 10 it can be seen that the amount of energy required to heat and evaporate a mixture of varying concentration of ammonia into water from 20°C until full evaporation is about 2400-2600 kJ/kg. Therefore it can be concluded that only a small amount of the cooling medium is evaporated.

4.2 Comparing Cooling Mediums

By studying Figure 15-Figure 20 it can be noted that the general behavior of switching from water to 25% NH3/75% H2O mixture as cooling medium, increases the cooling power throughout most of the test time.

Looking into Figure 21-Figure 23 shows similar results as in previous paragraph, i.e. a lower surface temperature of the HSU is achieved when using the 25% NH3/75% H2O mixture instead of water a spray-on cooling medium.

Figure 30 presents the total energy absorbed by each of the cooling mediums and at each setup. That table presents results illustrating that by using 25% NH3/75% H2O mixture instead of water as cooling medium, the cooling energy increases. A trend can also be seen that by increasing the initial test temperature [90°C; 120°C; 150°C] of the HSU, the efficiency of using 25% NH3/75% H2O mixture instead of water is increased, except for using the PJ20 nozzle at 150°C, which might be a measuring error.

By studying Figure 24-Figure 26 and the curves for PJ12 nozzle it can be seen that the 25% NH3/75% H2O mixture reduces the temperature more rapidly than water. However, when using the PJ20 nozzle no connection could be made regarding which medium is superior the other in sense of rate of temperature drop. This could be a result of the different flow rate of cooling medium applied by the two spray nozzles. By using the larger PJ20 nozzle the liquid might not have sufficient time to evaporate before being washed off the surface by subsequently sprayed coolant molecules which results in lower energy absorption.

5 Conclusion

The results show some promising benefits of using a mist of 25% NH3/75% H2O mixture as a spray-on cooling medium compared to pure water mist.

One benefit is that using the mixture instead of water allows the spray-on safety system to be operational in any application during sub-zero temperatures.

Using 25% NH3/75% H2O mixture instead of water presents an increase in cooling power and energy absorption when used as a spray-on cooling medium.

Switching nozzle from PJ20 to PJ12 (i.e. reducing the flow) shows an increase in energy absorption but a reduction in cooling power, given a specific volume of cooling medium, due to the difference in their flow rate and consequent spray duration.

By comparing the energy absorbed by the cooling medium during the physical tests with the simulation results it can be seen that the spray on liquid is not fully evaporated. This results an energy absorption lower than anticipated.

A higher flow rate offers a higher cooling power but it probably reduces the efficiency of utilizing evaporation for cooling since the coolant applied may be washed off the surface by subsequently sprayed coolant molecules before adequate heat transfer has been achieved. Reduced heat energy absorption is thus a consequence.

As described in the discussion section 4.2, the rate at which the cooling medium was applied may have been so high that the use of the coolant was not optimized. This could be solved by using some sort of pulse width modulated signal to control the flow of liquid, thereby allowing the same pressure, i.e. same droplet size, while decreasing the flow rate and thereby avoiding washing off the cooling liquid before it has evaporated.

One key downside of the chosen mixture is the fact that ammonia gas is toxic, which must not be neglected. When using 25% NH3/75% H2O mixture as a spray-on cooling medium the residues should be trapped or forcefully ventilated, so that toxic ammonia gas may not reach the vehicle passengers. If the gas were to be released to the surrounding of the vehicle, it should be diluted with water, e.g. by a subsequent water spraying unit.

One of the most interesting concept ideas coming out of this project is the observation that a cooling spray system might be able to function so as to hinder any cascading effects of thermal runaway between neighboring cells in a vehicle battery pack, i.e. work as an insulator for a limited time period. Hence, the spray-on cooling system potentially could work as an emergency cooling system that would postpone or even impede any thermal runaway that might take place in a battery system e.g. in a vehicle post-crash situation.

As described in 1.2.4.2 Air Cooling, batteries using air as cooling has spacing in between cells to allow air flow. The concept of a spray-on cooling system, as presented in this report, could be integrated into an air cooled battery system as an emergency cooling device dedicated to offer an increased safety margin against critical battery heat-up. The related risk for thermal runaway due to elevated heat exposure would thus be mitigated.

As presented in the section 4 Discussion, only minor predictable behavior is seen when investigating the relationship between nozzle hole diameter and cooling medium over a range of temperatures. The validation process of the concept safety system proposed in this project would benefit from having a larger test series being conducted in order to establish the true potentials and plausible benefits of using 25% NH_3/75% H_2O mixture as a spray-on cooling medium instead of pure water mist when thermally isolating a hot unit with a coolant.

While a mixture of ammonia and water has been considered throughout this project, any other mixture providing a multi-stage evaporation ability can be used as a spray-on cooling system for applications such as the battery emergency cooling concept described in early section 2 Method. The mixture should be chosen with consideration to the operational temperature of the unit to be cooled and its operational environment, e.g. if it is to be operated in winter climate the coolant's freezing point must be below the minimum temperature of the ambient, and its point of evaporation should be optimized so as to allow multi-step evaporation to start a the dedicated warning temperature of the battery unit.

6 Bibliography

Ashish Arora, N. K. M., Thomas Livernois, Jan Swart. (2010). Safety of Lithium-Ion Batteries for Hybrid Electric Vehicles. *Electric and Hybrid Vehicles*(First Edition), 29.

Aspen Technology, I. (2010). Physical Property Methods. Burlington, MA.

Axeon. (2012). Our Guide to Batteries. from http://www.axeon.com/getdoc/abb2a51a-ea57-416f-bdc4-79cbe7104d4f/Our-Guide-To-Batteries.aspx

B.V, E. (2013). Scopus. Retrieved 2013-06-11, 2013, from http://www.scopus.com

BETE. (2013). PJ-SMALLEST PHYSICAL SIZE / FINEST ATOMIZATION (pp. 85): BETE.

Castrol Perfecto HT5. (2009).

ENGINEERING, M. C. (2004). Thermophysical Properties of NH3 + H2O solutions for the industrial design of absorption refrigeration equipment. Zurich, Switzerland: M. CONDE ENGINEERING.

Festo. (2013). DSBF. In DSBF.JPG (Ed.). http://www.festo.com/net/no_no/SupportPortal/Press.aspx?cat=4213&tab=11&s=t: festo.

Hertzberg, T., Hahne, A., Josefsson, C., Holmstedt, G., & Husted, B. (2004). Brandforsk projekt 514-021

Kim, G. H., Gonder, J., Lustbader, J., & Pesaran, A. (2008). Thermal management of batteries in advanced vehicles using phase-change materials. *World Electric Vehicle Journal, 2*(2), 46-59.

Kistler. (2013). Kistler. Retrieved 2013-08-29, 2013, from http://www.kistler.com/

Kizilel, R., Sabbah, R., Selman, J. R., & Al-Hallaj, S. (2009). An alternative cooling system to enhance the safety of Li-ion battery packs. *Journal of Power Sources, 194*(2), 1105-1112. doi: http://dx.doi.org/10.1016/j.jpowsour.2009.06.074

Lisbona, D., & Snee, T. (2011). A review of hazards associated with primary lithium and lithium-ion batteries. *Process Safety and Environmental Protection, 89*(6), 434-442.

Lu, L., Han, X., Li, J., Hua, J., & Ouyang, M. (2013). A review on the key issues for lithium-ion battery management in electric vehicles. *Journal of Power Sources, 226*(0), 272-288. doi: http://dx.doi.org/10.1016/j.jpowsour.2012.10.060

Maleki, H., & Howard, J. N. (2009). Internal short circuit in Li-ion cells. *Journal of Power Sources, 191*(2), 568-574.

NIOSH (Producer). (1994, May). Immediately Dangerous To Life or Health (IDHL). *The National Institute for Occupational Safety and Health (NIOSH)*. Retrieved from http://www.cdc.gov/niosh/idlh/intridl4.html

Pesaran, A. A. (2001). *Battery Thermal Management in EVs and HEVs: Issues and Solutions*.

Pesaran, A. A. (2002). Battery thermal models for hybrid vehicle simulations. *Journal of Power Sources, 110*(2), 377-382. doi: http://dx.doi.org/10.1016/S0378-7753(02)00200-8

Place, B. (2011). How do the CO2 emissions from an electric car compare the a petrol car? (pp. 2). Australia: Better Place.

Products, A. (1999). MaterialSafetyDataSheets.

Rao, Z., & Wang, S. (2011). A review of power battery thermal energy management. *Renewable and Sustainable Energy Reviews, 15*(9), 4554-4571. doi: http://dx.doi.org/10.1016/j.rser.2011.07.096

Rao, Z., Wang, S., & Zhang, G. (2011). Simulation and experiment of thermal energy management with phase change material for ageing LiFePO4 power battery. *Energy Conversion and Management, 52*(12), 3408-3414. doi: http://dx.doi.org/10.1016/j.enconman.2011.07.009

Roth, E. P. (2008). Abuse Response of 18650 Li-Ion Cells with Different Cathodes Using EC:EMC/LiPF6 and EC:PC:DMC/LiPF6 Electrolytes. *ECS Transactions, 11*(19), 19-41. doi: 10.1149/1.2897969

Sahraei, E., Campbell, J., & Wierzbicki, T. (2012). Modeling and short circuit detection of 18650 Li-ion cells under mechanical abuse conditions. *Journal of Power Sources, 220*(0), 360-372. doi: http://dx.doi.org/10.1016/j.jpowsour.2012.07.057

Sahraei, E., Hill, R., & Wierzbicki, T. (2012). Calibration and finite element simulation of pouch lithium-ion batteries for mechanical integrity. *Journal of Power Sources, 201*(0), 307-321. doi: http://dx.doi.org/10.1016/j.jpowsour.2011.10.094

Sehlstedt, P. (2013). *Safety mechanisms for lithium ion batteries on cell level*. Gothenburg University. (06120-13-14646-1)

Shakhashiri, P. (2007). Gases of the air. from http://scifun.chem.wisc.edu/chemweek/pdf/airgas.pdf

Shimotake, H. (1990). *Progress in Batteries and Solar Cells*: JEC Press.

Smith, B. (2012). Chevrolet Volt Battery Incident Summary Report. Washington, DC: Office of Vehicle Safety Compliance NVS-224.

Spotnitz, R., & Franklin, J. (2003). Abuse behavior of high-power, lithium-ion cells. *Journal of Power Sources, 113*(1), 81-100.

Sturk, D. (2012). Risk Analysis From an EV/HEV collision point of view (pp. 33).

Team, M. E. V. (2008). A Guide to Understanding Battery Specifications.

Wikipedia. (2013). Thermocouple. Retrieved 2013-08-29, 2013, from http://en.wikipedia.org/wiki/Thermocouple

7 Appendix

Table 2, displays the full test series input configuration conducted during the physical testing.

Test	Purpose	Number of runs	Spray Fluid	Spray Pressure [Pa]	Test start temperature [C]	Nozzle Type	Distance Spray Nozzle-Battery Analog [m]
Test001	Cooling effect of spray-on water	1/2	Water	8,00E+05	90	PJ20	0,191
Test002	Cooling effect of spray-on water	2/2	Water	8,00E+05	90	PJ20	0,191
Test003	Cooling effect of spray-on water	1/2	Water	1,30E+06	90	PJ20	0,191
Test004	Cooling effect of spray-on water	2/2	Water	1,30E+06	90	PJ20	0,191
Test005	Cooling effect of spray-on water	1/2	Water	8,00E+05	120	PJ20	0,191
Test006	Cooling effect of spray-on water	2/2	Water	8,00E+05	120	PJ20	0,191
Test007	Cooling effect of spray-on water	1/2	Water	1,30E+06	120	PJ20	0,191
Test008	Cooling effect of spray-on water	2/2	Water	1,30E+06	120	PJ20	0,191
Test009	Cooling effect of spray-on water	1/2	Water	8,00E+05	150	PJ20	0,191
Test010	Cooling effect of spray-on water	2/2	Water	8,00E+05	150	PJ20	0,191
Test011	Cooling effect of spray-on water	1/2	Water	1,30E+06	150	PJ20	0,191
Test012	Cooling effect of spray-on water	2/2	Water	1,30E+06	150	PJ20	0,191
Test013	Cooling effect of spray-on water	1/2	Water	8,00E+05	90	PJ12	0,191
Test014	Cooling effect of spray-on water	2/2	Water	8,00E+05	90	PJ12	0,191
Test015	Cooling effect of spray-on water	1/2	Water	1,30E+06	90	PJ12	0,191
Test016	Cooling effect of spray-on water	2/2	Water	1,30E+06	90	PJ12	0,191
Test017	Cooling effect of spray-on water	1/2	Water	8,00E+05	120	PJ12	0,191
Test018	Cooling effect of spray-on water	2/2	Water	8,00E+05	120	PJ12	0,191
Test019	Cooling effect of spray-on water	1/2	Water	1,30E+06	120	PJ12	0,191
Test020	Cooling effect of spray-on water	2/2	Water	1,30E+06	120	PJ12	0,191
Test021	Cooling effect of spray-on water	1/2	Water	8,00E+05	150	PJ12	0,191
Test022	Cooling effect of spray-on water	2/2	Water	8,00E+05	150	PJ12	0,191
Test023	Cooling effect of spray-on water	1/2	Water	1,30E+06	150	PJ12	0,191
Test024	Cooling effect of spray-on water	2/2	Water	1,30E+06	150	PJ12	0,191
Test025	Cooling effect of spray-on Ammonia/Water	1	Ammonia/Water Mix	1,30E+06	90	PJ20	0,191
Test026	Cooling effect of spray-on Ammonia/Water	1	Ammonia/Water Mix	1,30E+06	120	PJ20	0,191
Test027	Cooling effect of spray-on Ammonia/Water	1	Ammonia/Water Mix	1,30E+06	150	PJ20	0,191
Test028	Cooling effect of spray-on Ammonia/Water	1	Ammonia/Water Mix	1,30E+06	90	PJ12	0,191
Test029	Cooling effect of spray-on Ammonia/Water	1	Ammonia/Water Mix	1,30E+06	120	PJ12	0,191
Test030	Cooling effect of spray-on Ammonia/Water	1	Ammonia/Water Mix	1,30E+06	150	PJ12	0,191

Table 3, displays the output data with observation comments from the testing.

Test	Comments	Initial	Final after spray	Final	Total Test Time [s]
		Temperature [°C]			
Test001	Large droplets on battery analog after test	90	83,8	81,8	250
Test002	Large droplets on battery analog after test	90	83,8	81,8	250
Test003	Large droplets on battery analog after test	90	84,7	81,9	250
Test004	Large droplets on battery analog after test	90	84,8	82,1	250
Test005	Very few, large, droplets on battery analog after test	120	110,5	107,8	250
Test006	Very few, large, droplets on battery analog after test	120	110,4	107,7	250
Test007	Very few, large, droplets on battery analog after test	120	112	108,3	250
Test008	Very few, large, droplets on battery analog after test	120	111,7	108,2	250
Test009	Steam, No droplets on battery analog	150	136,8	133,2	250
Test010	Steam, No droplets on battery analog	150	137,1	133,7	250
Test011	Steam, No droplets on battery analog	150	138,6	134	250
Test012	Steam, No droplets on battery analog	150	138,4	134,1	250
Test013	Large droplets on battery analog after test	90	80,2	78,8	600
Test014	Large droplets on battery analog after test	90	80,2	78,7	600
Test015	Large droplets on battery analog after test	90	80,2	79,3	400
Test016	Large droplets on battery analog after test	90	80,2	79,3	400
Test017	Very few, large, droplets on battery analog after test	120	104,7	102,3	600
Test018	Very few, large, droplets on battery analog after test	120	104,7	102,4	600
Test019	Very few, large, droplets on battery analog after test	120	104,8	103,6	400
Test020	Very few, large, droplets on battery analog after test	120	104,8	103,7	400
Test021	Steam, No droplets on battery analog	150	132	129,8	600
Test022	Steam, No droplets on battery analog	150	132,5	130,5	600
Test023	Steam, No droplets on battery analog	150	131	129,5	400
Test024	Steam, No droplets on battery analog	150	132,5	131	400
Test025	Some large droplets on analog. Blue liquid around brass parts, intense odor 5m radius	90	83,6	80,6	250
Test026	No droplets, no blue liquid anymore(not as much atleast)	120	110,3	105,8	250
Test027	No droplets, copper no longer gold-colored, blue liquid at copper.	150	139,5	135,4	250
Test028	Some large droplets on analog. Blue liquid around brass parts, intense odor 5m radius	90	79,8	78,4	400
Test029	No droplets, no blue liquid anymore(not as much atleast)	120	102,8	100,7	400
Test030	No droplets, copper no longer gold-colored, blue liquid at copper.	150	127,6	125,4	400

CHALMERS, *Applied Mechanics*, Master's Thesis 2013:

Table 4, displays the tests performed to find the heat radiation from the HSU to the environment.

Test	Purpose	Number of runs	Initial Temperature[C]	Cooling Time [s]	Final Temp after Cooling time [C]
Test0C1	Heat contribution from oil pump and heat radiation to surrounding	1/6	90	600	86,8
Test0C2	Heat contribution from oil pump and heat radiation to surrounding	2/6	90	600	87,3
Test0C3	Heat contribution from oil pump and heat radiation to surrounding	3/6	119,9	600	114,7
Test0C4	Heat contribution from oil pump and heat radiation to surrounding	4/6	119,9	600	115,1
Test0C5	Heat contribution from oil pump and heat radiation to surrounding	5/6	150	600	143,2
Test0C6	Heat contribution from oil pump and heat radiation to surrounding	6/6	150	600	143,9

CHALMERS, *Applied Mechanics*, Master's Thesis 2013: